

# IQ-Aware Precoding for Atomic MIMO Receivers

Mingyao Cui, *Graduate Student Member, IEEE*, Qunsong Zeng, *Member, IEEE*, and Kaibin Huang, *Fellow, IEEE*

**Abstract**—Leveraging the strong atom-light interaction, Rydberg atomic receivers significantly enhance the sensitivity of electromagnetic signal measurements, outperforming traditional antennas. Existing research primarily focuses on improving the architecture and signal detection algorithms of atomic receivers, while established signal processing schemes at the transmitter end have remained constant. However, these schemes fail to maximize the throughput of atomic receivers due to the non-linearity of transmission model. To address this issue, our work represents the first attempt to design transmitter precoding in multiple-input multiple-output systems to achieve the capacity of atomic receivers. Specifically, we initially harness a strong reference approximation to convert the *nonlinear magnitude-detection* model of atomic receivers into a *linear real-part detector*. Based on this approximation, we prove that the degree of freedom is  $\min\{N_r/2, N_t\}$  for a point-to-point MIMO system comprising an  $N_r$ -antenna atomic receiver and an  $N_t$ -antenna classic transmitter. To achieve the system capacity, we propose an IQ-aware fully digital precoding method. Unlike traditional complex-valued digital precoders that jointly manipulate the in-phase and quadrature (IQ) symbols, our method employs four real matrices to independently precode the IQ baseband symbols. This method is demonstrated to be optimal for atomic receivers. In addition, to eliminate the reliance on fully digital precoding architecture, we further explore IQ-aware hybrid precoding techniques. Our design incorporates a low-dimensional IQ-aware digital precoder and a high-dimensional complex analog precoder, implemented by either fully-connected or sub-connected phase shifters networks. Alternating minimization algorithms are proposed to produce the IQ-aware hybrid precoders, with the objective of closely approximating the optimal IQ-aware fully digital precoder. Simulation results validate the superiority of proposed IQ-aware precoding methods over existing techniques in atomic-receiver enabled MIMO communications.

**Index Terms**—Atomic receivers, multiple-input-multiple-output (MIMO), precoding, quantum sensing.

## I. INTRODUCTION

Ever since Hertz validated the existence of electromagnetic (EM) waves, the accurate measurement of EM waves has become the cornerstone of modern wireless communication, remote sensing, and radar [1], [2]. To date, a variety of antenna technologies have been developed, including but not limited to dipole antennas and aperture antennas. These technologies are based on a universal measurement principle, where the incident EM wave drives the antenna to generate induced currents, resulting in informative electrical signals. Although this mechanism has been used for over half a century, it imposes a notable limitation to the sensitivity (i.e., minimum detectable field strength) of traditional antennas. According to the fluctuation-dissipation theorem [3], the random movement

of free electrons within metal generates indistinguishable thermal noise, known as Johnson-Nyquist noise, that contaminates electrical signals. As a result, traditional antennas typically achieve a sensitivity on the order of  $1\text{mV/cm}/\sqrt{\text{Hz}}$ , making ultra-precise EM-field measurement challenging to achieve [4], [5].

Recently, at the intersection of quantum sensing and wireless communication, an emerging antenna technology known as *Rydberg atomic receivers* has demonstrated the potential in surpassing the sensitivity limitations of traditional antennas [6], [7]. Rydberg atoms, highly excited atoms operating at high quantum states [8], possess large electric dipole moments. These atoms can strongly interact with incident EM waves, triggering electron transitions between resonant energy levels [9]. Receivers based on Rydberg atoms can monitor the strength of these transitions by leveraging quantum phenomena, such as *ac-Stark shift* and *electromagnetically induced transparency* (EIT), facilitating the detection of information-carrying EM fields [7]. This paradigm shift in EM field measurement mechanisms allows Rydberg atomic receivers to overcome the measurement limitations imposed by thermal noise, as the interaction between EM fields and atoms theoretically introduces no thermal noise. Furthermore, the quantum shot noise induced during the observation of Rydberg atoms' quantum states is typically orders of magnitude smaller than the thermal noise of metal antennas [10]. With these advantages, atomic receivers has been reported to achieve measurement sensitivity on the order of  $5\text{nV/cm}/\sqrt{\text{Hz}}$  [11]. Thereafter, Rydberg atomic receivers show promise for use in long-range communication scenarios, such as satellite communications and space-air-ground networks [12], where detecting weak electric signals is crucial. Aligned with this vision, our work advocates the adoption of atomic receivers as a revolutionary approach to enhance wireless communication systems.

Existing research on the application of Rydberg atomic receivers in detecting informative wireless signals primarily focused on the lab demonstration of *single-input single-output* (SISO) air interfaces. Specifically, through the interaction between EM fields and Rydberg atoms, the strength and frequency of EM waves are transduced into the intensity of electron transition, termed the *Rabi frequency*. By inferring symbols from Rabi frequency, researchers have successfully demonstrated the detection of amplitude-modulated (AM) and frequency-modulated (FM) signals [13]–[15]. To enable phase modulation, techniques such as holographic phase-sensing or quantum superheterodyne detection have been employed [16]. These techniques utilize a *local oscillator* (LO) to send a known reference wave that interferes with the signal wave, thereby allowing phase-modulated symbols to be extracted from the phase difference between the two waves. This method

M. Cui, Q. Zeng, and K. Huang are with the Department of Electrical and Electronic Engineering, The University of Hong Kong, Hong Kong (Email: {mycui, qszeng, huangk} @eee.hku.hk). Corresponding authors: Q. Zeng; K. Huang.

has facilitated the reception of *phase-shift keying* (PSK) and *quadrature-amplitude modulation* (QAM) symbols in communication systems [17]–[19], as well as the detection of microvibration in WiFi-sensing systems [10]. Another representative application involves the concurrent detection of multi-frequency signals spanning approximately GHz frequency bands [20]–[22]. This is achieved either by mixing different species of alkali atoms within a single receiver or by triggering the atoms to distinct Rydberg states.

In addition to the SISO air interface, recent studies have also explored the spatial diversity and multiplexing gains of atomic receivers using Rydberg atom-based antenna arrays. In [23], a *single-input multiple-output* (SIMO) pipeline was established, deploying four atomic antennas to recover AM signals. A notable observation from this study was that the experimental receive *signal-to-noise ratio* (SNR) scales linearly with the number of atomic antennas, as expected. This atomic SIMO configuration was later implemented for angle-of-arrival estimation using the holographic phase-sensing scheme [24], [25]. To further reap the multiplexing gain, our prior work developed a multi-user signal detection model for atomic *multiple-input multiple-output* (MIMO) receivers [26]. We proved that atomic MIMO receivers exhibit a *non-linear* input-output relationship modeled by *biased phase retrieval* [27], in contrast to the *linear transition model* in classic MIMO systems. Subsequently, a maximum likelihood-based algorithm was proposed for the simultaneous detection of multi-user signals.

Notably, previous efforts have primarily concentrated on improving the receiver architectures and detection algorithms, while the design of a classic transmitter capable of seamlessly collaborating with an atomic receiver remains largely uncharted. In fact, attributed to the altered input-output relationship, existing transmitter-side signal processing methods may not be optimal for atomic receivers. For instance, classic MIMO communications rely on *singular value decomposition* (SVD)-based precoding at the transmitter side to achieve the capacity limit  $\min\{N_r, N_t\} \log \text{SNR}$ , where  $N_r$  and  $N_t$  represent the number of antennas at the receiver and transmitter, respectively [28], [29]. However, this capacity is based on the *linear transition model*, which is not suitable for the *non-linear transition model* established in atomic MIMO systems. This observation raises three critical questions that remain unaddressed in existing literature:

- *What is the information-theoretical limit of an atomic MIMO receiver?*
- *How can we approach this limit through transmitter-side signal processing?*
- *Is there any loss in degree-of-freedom (DoF) in atomic MIMO systems due to the non-linear transition?*

Addressing these questions is of pivotal significance for the seamless integration of atomic receivers into next-generation communication systems.

To fill in this gap, this work represents the first attempt at analyzing and designing the transmitter precoding to approach the information-theoretic limit of Rydberg atomic MIMO systems. We consider the point-to-point MIMO communications

supported by the holographic phase-sensing measurement scheme. The key contributions are summarized as follows.

- **Mutual information of atomic MIMO systems:** We propose a strong-reference approximation to analyze the mutual information of atomic MIMO systems. This approximation is motivated by the observation that the reference wave is much stronger than the signal wave, as LOs are typically deployed near atomic receivers [17]–[19]. By discarding higher-order infinitesimal quantities, the *non-linear magnitude detection model* of atomic receivers can be linearized to a *real-part detection* model, allowing us to express the mutual information analytically. We then prove that the corresponding ergodic capacity scales as  $\min\{N_r/2, N_t\} \log \text{SNR}$  at high SNRs with a DoF of  $\min\{N_r/2, N_t\}$ . This capacity limit indicates that as long as the number of atomic antennas is at least twice the number of transmit antennas, atomic MIMO systems experience no DoF loss compared to traditional counterparts, regardless of the absence of the imaginary part information.
- **IQ-aware digital precoding:** An IQ-aware digital precoding method is proposed to achieve the instantaneous capacity of atomic receivers for each channel realization. In classic MIMO systems, complex-valued digital precoders can achieve the system capacity by *jointly* processing the in-phase and quadrature (IQ) baseband symbols using the real and imaginary components of the precoder. However, we show that the complex-valued digital precoder is not optimal for atomic receivers due to the absence of the imaginary part of the received signal. In contrast, our IQ-aware digital precoder employs *four* real-valued matrices to *independently* precode the IQ baseband symbols before entering the IQ modulator. This offers more flexible manipulation on the distribution of radiated signals. Subsequently, by harnessing the SVD of the equivalent real-valued wireless channel, we demonstrate that an IQ-aware digital precoder achieves the instantaneous capacity of atomic receivers, with a maximal DoF of  $\min\{N_r/2, N_t\}$ .
- **IQ-aware hybrid precoding:** Despite the capacity-achieving property of IQ-aware digital precoder, it relies on a fully digital precoding architecture since analog radio-frequency (RF) circuits cannot independently process the IQ symbols. To eliminate this reliance, we further investigate the IQ-aware hybrid precoding technique, which incorporates a low-dimensional IQ-aware digital precoder realized by a baseband processor and a high-dimensional complex analog precoder realized by *phase shifters* (PSs). Our design focuses on two typical hybrid precoding architecture: the fully-connected (FC) and the sub-connected (SC) PS networks. We exploit the alternating minimization approach to alternatively update the digital and analog precoders, with the objective of minimizing the Frobenius distance between the IQ-aware fully digital precoder and the designed IQ-aware hybrid precoder. Numerical results validate that the FC IQ-aware hybrid precoder can closely approach the optimal

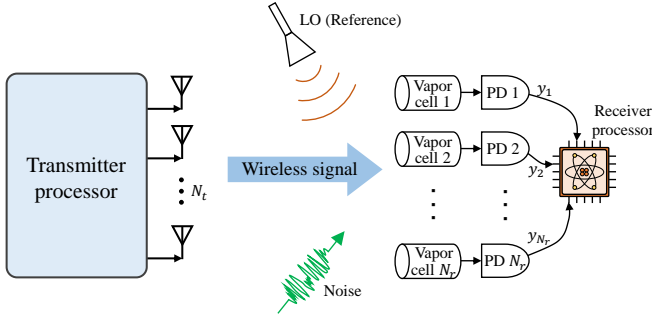


Figure 1. Layout of the Rydberg atomic MIMO system.

IQ-aware digital precoder. Moreover, we show that the proposed IQ-aware hybrid precoding schemes significantly outperform classical hybrid precoding methods in atomic-receiver based MIMO systems, demonstrating the effectiveness of the proposed designs.

*Organization:* The remainder of this paper is organized as follows. The system model of atomic MIMO receivers is provided in Section II. In Section III, we analyze the mutual information of atomic receivers and the limit of ergodic capacity. The IQ-aware fully digital precoding for achieving the instantaneous capacity is discussed Section IV. The IQ-aware hybrid precoding for the FC and SC architectures are elaborated in Section V. In Section VI, we validate the proposed design by numerical results. Finally, conclusions are drawn in Section VII.

*Notations:* Lower-case and upper-case boldface letters represent vectors and matrices, respectively.  $\mathbf{X}_{m,n}$ ,  $\mathbf{X}_{m,:}$ , and  $\mathbf{X}_{:,n}$  represent the  $(m,n)$ -th entry, the  $m$ -th row, and the  $n$ -th column of matrix  $\mathbf{X}$ , respectively. Moreover,  $\mathbf{X}_{m:n,:}$  and  $\mathbf{X}_{:,m:n}$  are defined as the  $m$  to  $n$  columns and  $m$  to  $n$  rows of  $\mathbf{X}$ .  $[\cdot]^{-1}$ ,  $[\cdot]^{\dagger}$ ,  $[\cdot]^*$ ,  $[\cdot]^T$ , and  $[\cdot]^H$  denote the inverse, pseudo-inverse, conjugate, transpose, and conjugate-transpose operations, respectively.  $\|\cdot\|_2$  denotes the  $l_2$ -norm of the argument.  $\|\cdot\|_F$  denotes the Frobenius norm of the argument.  $|\cdot|$  denotes the element-wise magnitude of its argument.  $\text{Tr}(\cdot)$  denotes the trace operator.  $\mathbb{E}(\cdot)$  is the expectation operator.  $\text{Re}(\cdot)$  denotes the real part of the argument.  $\arg(\cdot)$  is the phase of the argument.  $\mathcal{CN}(\boldsymbol{\mu}, \boldsymbol{\Sigma})$  ( $\mathcal{N}(\boldsymbol{\mu}, \boldsymbol{\Sigma})$ ) denotes the complex (real) Gaussian distribution with mean  $\boldsymbol{\mu}$  and covariance  $\boldsymbol{\Sigma}$ .  $\mathcal{U}(a, b)$  denotes the uniform distribution between  $a$  and  $b$ .  $\mathbf{I}_L$  is an  $L \times L$  identity matrix.

## II. REVIEW OF RYDBERG ATOMIC MIMO SYSTEM

We consider an atomic MIMO communication system, as illustrated in Fig. 1. The transmitter employs a conventional  $N_t$ -element antenna array for data transmission. The time-domain radiated signal from the  $n$ -th antenna,  $n \in \{1, 2, \dots, N_t\}$ , is represented as  $x_n(t) = A_n \cos(\omega t + \gamma_n)$ . To realize phase demodulation at the receiver side, we adopt the holographic-phase sensing measurement, where a LO is introduced to radiate predetermined reference signals to the atomic receiver. Let the reference signal,  $x_R(t)$ , share the same frequency with the transmitted signal, and thereby it is expressed as  $x_R(t) = A_R \cos(\omega t + \gamma_R)$ .

The atomic receiver deploys  $N_r$  Rydberg atomic antennas for detecting the wireless signals. Each atomic antenna consists of a vapor cell filled with Alkali atoms, followed by a photodetector (PD). These atoms are excited to Rydberg states for sensing the incident EM wave via atom-light interaction, while the sensing results are read out by PDs [30]. Adopting the multi-path wireless channel model, the EM wave,  $\mathbf{E}_m(t)$ , impinging on the  $m$ -th atomic antenna,  $m \in \{1, 2, \dots, N_r\}$ , is written as

$$\mathbf{E}_m(t) = \sum_{n=1}^{N_t} \sum_{\ell=1}^L \epsilon_{mnl} \rho_{mnl} A_n \cos(\omega t + \varphi_{mnl} + \gamma_n) + \epsilon_{R,m} \rho_{R,m} A_R \cos(\omega t + \varphi_{R,m} + \gamma_R). \quad (1)$$

Here,  $L$  denotes the number of paths between the transmitter and receiver. Variables  $\epsilon_{mnl}$ ,  $\rho_{mnl}$ , and  $\varphi_{mnl}$  represent the polarization direction, path loss, and phase shift of the propagation from the  $n$ -th transmit antenna to the  $m$ -th atomic antenna via the  $\ell$ -th path. Besides, variables  $\epsilon_{R,m}$ ,  $\rho_{R,m}$ , and  $\varphi_{R,m}$  refer to the channel parameters pertaining to the reference signal. Since the LO is typically deployed nearby the receiver, we directly employ the line-of-sight path to model the LO-to-receiver channel. Suppose the signal frequency of the incident EM wave,  $\omega$ , is tuned resonant with the transition frequency between the ground and excited energy levels of Rydberg atoms. Governed by the time-dependent Schrödinger equation [31], the electrons will oscillate between the ground and excited energy levels, a phenomenon referred to as electron transition. The intensity of electron transition is determined by the Rabi frequency [31],  $\Omega_m$ , given as

$$\Omega_m = \frac{|\boldsymbol{\mu}_{\text{RF}}^T \mathbf{E}_{\text{RF},m}|}{\hbar}. \quad (2)$$

where  $\boldsymbol{\mu}_{\text{RF}}$  represents the electric dipole moment between Rydberg states, and  $\hbar$  denotes the reduced Planck constant. Applying the rotating wave approximation [31], our prior work [26] proved that the vector  $\mathbf{E}_{\text{RF},m}$  can be equivalently expressed as the down-converted complex form of  $\mathbf{E}_m(t)$ , i.e.,

$$\mathbf{E}_{\text{RF},m} = \sum_{n=1}^{N_t} \sum_{\ell=1}^L \epsilon_{mnl} \rho_{mnl} A_n e^{j(\varphi_{mnl} + \gamma_n)} + \epsilon_{R,m} \rho_{R,m} A_R e^{j(\varphi_{R,m} + \gamma_R)}, \quad (3)$$

where the frequency,  $\omega$ , is cancelled due to electron transition. Given that the wireless signals are embedded into Rabi frequencies,  $\{\Omega_m\}$ , accurate signal detection hinges on measuring their values using practical implementations, such as the EIT effects. Specifically, the electron transition of Rydberg atoms changes the susceptibility of the vapor cell [7]. By steering a probe laser to penetrate through the vapor cell and observing the dynamic change of its spectrum using a PD, the Rabi frequency can be read out. We denote the measurement of  $[\Omega_1, \dots, \Omega_{N_r}]^T$  as a vector,  $\mathbf{y} = [y_1, \dots, y_{N_r}]^T$ , followed by

$$\mathbf{y} = \mathbf{H}\mathbf{x} + \mathbf{r}. \quad (4)$$

Here,  $\mathbf{H} \in \mathbb{C}^{N_r \times N_t}$  represents the effective channel, with the  $(m,n)$ -th entry given as

$\mathbf{H}_{m,n} = \sum_{\ell=1}^L \frac{1}{\hbar} \boldsymbol{\mu}_{\text{RF}}^T \boldsymbol{\epsilon}_{mnl} \rho_{mnl} e^{j\varphi_{mnl}}$ , the vector  $\mathbf{x} = [x_1, x_2, \dots, x_{N_t}]^T$  with  $x_n = A_n e^{j\gamma_n}$  denotes the transmitted signal in the complex form, and  $\mathbf{r} = [r_1, r_2, \dots, r_{N_r}]^T$  with  $r_m = \frac{1}{\hbar} \boldsymbol{\mu}_{\text{RF}}^T \boldsymbol{\epsilon}_{R,m} \rho_{R,m} A_R e^{j(\varphi_{R,m} + \gamma_R)}$ , denotes the received reference signal.

Finally, by invoking the law of large numbers, the measurement noise can be modelled as the circularly symmetric Gaussian distribution,  $\mathbf{w} \sim \mathcal{CN}(0, \sigma^2 \mathbf{I}_{N_r})$ . As a result, we arrive at the following input-output relationship for atomic MIMO systems:

$$\mathbf{y} = |\mathbf{H}\mathbf{x} + \mathbf{r} + \mathbf{w}|, \quad (5)$$

which is a non-linear magnitude-detection model. To analyze the achievable capacity,  $C$ , of Rydberg receivers, this article focuses on the transmitter design to maximize the mutual information between  $\mathbf{y}$  and  $\mathbf{x}$ :

$$C = \max_{p(\mathbf{x})} \mathcal{I}(\mathbf{y}; \mathbf{x}) = \mathcal{H}(\mathbf{y}) - \mathcal{H}(\mathbf{y}|\mathbf{x}), \quad (6)$$

where  $\mathcal{H}(\cdot)$  denotes the entropy of its arguments and  $\mathcal{I}(\cdot; \cdot)$  the mutual information of its arguments.

### III. MUTUAL INFORMATION OF ATOMIC MIMO SYSTEMS

In this section, we introduce a *strong reference approximation* to linearize the non-linear transition model in (5), built on which the mutual information,  $\mathcal{I}(\mathbf{y}; \mathbf{x})$ , is explicitly formulated. We then analyze the DoF of atomic MIMO systems relying on the modeled mutual information.

#### A. Approximated Mutual Information

It is evident from (5) that the atomic receiver exhibits a non-linear input-output relationship, given that Rabi frequencies,  $\{\Omega_m\}$ , only capture the magnitude of incident EM waves. This fact makes it intractable to express the mutual information,  $\mathcal{I}(\mathbf{y}; \mathbf{x})$ , analytically, let alone maximizing it. To overcome this challenge, we note that the artificially introduced LOs are typically placed close to the atomic receiver in practical implementations [17]–[19], [32]. In particular, the LO-to-receiver distance is almost tens of centimeters, which is significantly shorter than the transmitter-to-receiver distance. Considering the quadratic-scaling path loss [33], *the reference signal can be much stronger than the wireless data and noise*. This strong reference approximation allows us to linearize the transmission model in (5) as follows.

**Proposition 1.** (*Strong reference approximation*): If each entry of the reference signal is greatly stronger than the wireless data and noise, i.e.,

$$|r_m| \gg |\mathbf{H}_{m,:} \mathbf{x} + w_m|, \quad (7)$$

then we can approximate  $\mathbf{y}$  as

$$\tilde{\mathbf{y}} = \mathbf{y} - |\mathbf{r}| \approx \text{Re}(\tilde{\mathbf{H}}\mathbf{x}) + \mathbf{w}_I, \quad (8)$$

where  $\mathbf{w}_I \sim \mathcal{N}(0, \frac{\sigma^2}{2} \mathbf{I}_{N_r})$  and  $\tilde{\mathbf{H}}_{m,:} \triangleq e^{-j\angle r_m} \mathbf{H}_{m,:}$ .

*Proof:* (See Appendix A).  $\square$

Proposition 1 indicates that, in the strong-reference-signal regime, the *non-linear* magnitude detector in (5) can be transformed into a *linear* real-part detector in (8) by subtracting the offset  $|\mathbf{r}|$ . More importantly, the complicated mutual information,  $\mathcal{I}(\mathbf{y}; \mathbf{x}) = \mathcal{I}(\tilde{\mathbf{y}}; \mathbf{x})$ , is converted to a tractable expression:

$$\mathcal{I}(\tilde{\mathbf{y}}; \mathbf{x}) \rightarrow \mathcal{I}(\text{Re}(\tilde{\mathbf{H}}\mathbf{x}) + \mathbf{w}_I; \mathbf{x}). \quad (9)$$

To further simplify (8) and (9), we introduce the subscript  $I$  and  $Q$  to denote the real (in-phase) and imaginary (quadrature) components of a complex number, e.g.,  $\tilde{\mathbf{H}} = \tilde{\mathbf{H}}_I + j\tilde{\mathbf{H}}_Q$  and  $\mathbf{x} = \mathbf{x}_I + j\mathbf{x}_Q$ . Then, the received signal  $\tilde{\mathbf{y}}$  is rewritten as

$$\tilde{\mathbf{y}} = \underbrace{(\tilde{\mathbf{H}}_I, -\tilde{\mathbf{H}}_Q)}_{\tilde{\mathbf{H}}} \underbrace{\begin{pmatrix} \mathbf{x}_I \\ \mathbf{x}_Q \end{pmatrix}}_{\tilde{\mathbf{x}}} + \mathbf{w}_I, \quad (10)$$

where  $\tilde{\mathbf{H}} \in \mathbb{R}^{N_r \times 2N_t}$  and  $\tilde{\mathbf{x}} \in \mathbb{R}^{2N_t \times 1}$  are defined as the equivalent *real-valued* channel and radiated signal, respectively. Attributed to the linear behavior of real-part detectors, the maximal throughput is achieved when the radiated signal  $\tilde{\mathbf{x}}$  follows the Gaussian distribution  $\tilde{\mathbf{x}} \sim \mathcal{N}(0, \mathbf{Q})$ , with the covariance matrix  $\mathbf{Q} = \text{E}(\tilde{\mathbf{x}}\tilde{\mathbf{x}}^T) \in \mathbb{R}^{2N_t \times 2N_t}$ . Thereafter, the mutual information is expressed as

$$\mathcal{I}(\text{Re}(\tilde{\mathbf{H}}\mathbf{x}) + \mathbf{w}_I; \mathbf{x}) = \frac{1}{2} \log \det \left( \mathbf{I}_{N_r} + \frac{2}{\sigma^2} \tilde{\mathbf{H}}\mathbf{Q}\tilde{\mathbf{H}}^T \right). \quad (11)$$

Here, the discount factor  $\frac{1}{2}$  arises because the variables  $\tilde{\mathbf{H}}$ ,  $\tilde{\mathbf{x}}$ , and  $\mathbf{w}_I$  are all real valued. Moreover, considering the total power constraint imposed on the radiated signal, we have

$$\text{Tr}\{\text{E}(\mathbf{x}\mathbf{x}^H)\} = \text{Tr}\{\text{E}(\tilde{\mathbf{x}}\tilde{\mathbf{x}}^T)\} = \text{Tr}\{\mathbf{Q}\} = P, \quad (12)$$

where  $P$  is the transmission power. In summary, leveraging the strong reference approximation, the achievable capacity,  $C$ , in (6) can be reformulated as

$$C = \max_{\substack{\text{Tr}\{\mathbf{Q}\}=P, \\ \mathbf{Q} \succeq 0}} \frac{1}{2} \log \det \left( \mathbf{I}_{N_r} + \frac{2}{\sigma^2} \tilde{\mathbf{H}}\mathbf{Q}\tilde{\mathbf{H}}^T \right). \quad (13)$$

The major difference between the mutual information (13) and that of the conventional MIMO [28] is due to the conversion of channel matrix and covariance matrix from their complex form to real form, i.e.,  $\mathbf{H} \in \mathbb{C}^{N_r \times N_t} \Rightarrow \tilde{\mathbf{H}} \in \mathbb{C}^{N_r \times 2N_t}$  and  $\mathbf{Q} = \text{E}(\mathbf{x}\mathbf{x}^H) \Rightarrow \tilde{\mathbf{Q}} = \text{E}(\tilde{\mathbf{x}}\tilde{\mathbf{x}}^T)$ . Therefore, the transmission model (8) prefers real-valued matrix manipulation, rather than complex-valued one.

#### B. Degree-of-Freedom Analysis

It is well-known that, at high SNR, the ergodic capacity of a conventional MIMO system is  $\min\{N_r, N_t\} \log \frac{\text{SNR}}{N_t} + \mathcal{O}(1)$ , where  $\min\{N_r, N_t\}$  signifies the system's DoF, and the average SNR is defined as  $\text{SNR} = \frac{P}{\sigma^2}$  (see [28], [29]). Following the same analysis method, we will study the ergodic capacity of atomic MIMO receivers and the corresponding DoF based on the transition model (8).

The channel state information (CSI) is assumed to be known to the receiver, but not at the transmitter [29]. Given this assumption, the covariance matrix of radiated signal should

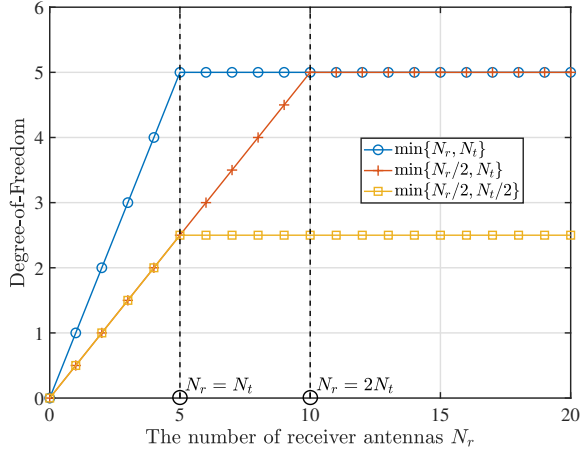


Figure 2. Comparison between the three DoFs:  $\frac{1}{2} \min\{N_r, N_t\}$ ,  $\min\{\frac{N_r}{2}, N_t\}$ , and  $\min\{N_r, N_t\}$ , where  $N_t = 5$ .

have a uniform power allocation, i.e.,  $\bar{\mathbf{Q}} = \frac{P}{2N_t} \mathbf{I}_{2N_t}$ . We assume that the coefficients of  $\mathbf{H}$  follow an independent and identical distributed (i.i.d) complex circularly symmetric Gaussian distribution with unit variance. The ergodic capacity of this transmission model is then obtained by averaging  $\mathbf{H}$  (or  $\bar{\mathbf{H}}$ ):

$$C_e = \mathbb{E} \left[ \frac{1}{2} \log \det \left( \mathbf{I}_{N_r} + \frac{\text{SNR}}{N_t} \bar{\mathbf{H}} \bar{\mathbf{H}}^T \right) \right]. \quad (14)$$

Following the standard analysis of MIMO channel capacity, the asymptotic behavior of  $C_e$  at high SNRs is derived below.

**Proposition 2.** At high SNRs, the ergodic capacity,  $C_e$ , is asymptotically

$$C_e = \min \left\{ \frac{N_r}{2}, N_t \right\} \log \frac{\text{SNR}}{N_t} + \mathcal{O}(1), \quad (\text{SNR} \rightarrow \infty). \quad (15)$$

*Proof:* (See Appendix B).  $\square$

Proposition 2 suggests that the transmission rate of atomic MIMO system is improved by  $\min\{N_r/2, N_t\}$  bit/s/Hz for every 3 dB increment in SNR, which corresponds to a DoF of  $\lim_{\text{SNR} \rightarrow \infty} \frac{C_e}{\log \text{SNR}} = \min\{\frac{N_r}{2}, N_t\}$ . This result is attributed to the fact that the DoF is lost at the receiver side due to the absence of imaginary-part information, while the DoF remains intact at the transmitter side. Thereafter, a discount factor  $\frac{1}{2}$  is imposed on  $N_r$ , giving rise to a DoF of  $\min\{\frac{N_r}{2}, N_t\}$ . To clarify our discussion, we compare three DoFs,  $\min\{N_r, N_t\}$ ,  $\min\{\frac{N_r}{2}, N_t\}$ , and  $\frac{1}{2} \min\{N_r, N_t\}$ , as a function of  $N_r$  in Fig. 2. These three DoFs have their own physical meaning: the former two refer to DoFs of conventional MIMO and atomic MIMO systems, while the last one is interpreted as the DoF of *real-valued symbols* transmission on the in-phase channel.

As  $N_r$  increases, the DoF  $\min\{\frac{N_r}{2}, N_t\}$  gradually climbs from  $\frac{1}{2} \min\{N_r, N_t\}$  to  $\min\{N_r, N_t\}$ . Specifically, when  $N_r < N_t$ , we have  $\min\{\frac{N_r}{2}, N_t\} = \frac{1}{2} \min\{N_r, N_t\} = \frac{1}{2} N_r$ . The DoF of atomic MIMO systems is exactly half of that of conventional systems. In this context, it is sufficient to

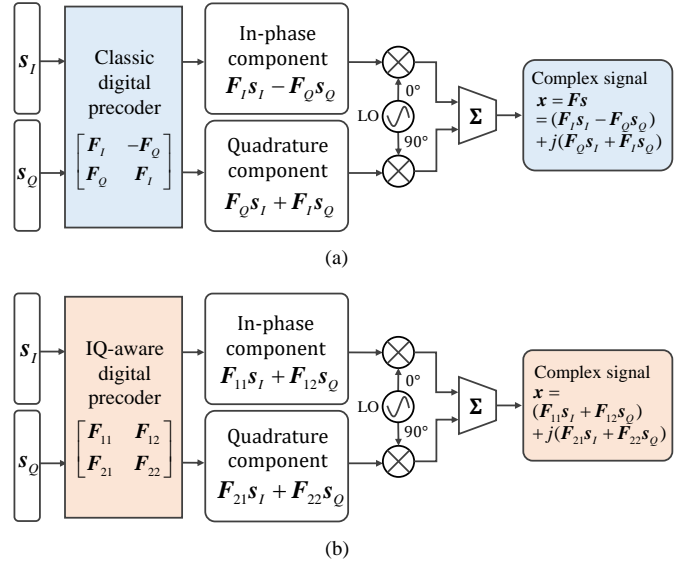


Figure 3. (a) The classic complex digital precoding and (b) the proposed IQ-aware digital precoding.

achieve the capacity of atomic receivers by transmitting  $\frac{N_r}{2}$  complex-valued symbols, or equivalently,  $N_r$  real-valued symbols on the in-phase channel only. Moreover, as  $N_r$  grows from  $N_t$  to  $2N_t$ , the DoF,  $\min\{N_r, N_t\}$ , get saturated while the gap between  $\min\{N_r, N_t\}$  and  $\min\{N_r/2, N_t\}$  narrows. Particularly, when  $N_r \geq 2N_t$ , we have  $\min\{\frac{N_r}{2}, N_t\} = \min\{N_r, N_t\} = N_t$ . This implies that an atomic receiver does not suffer any DoF loss compared to its traditional counterpart if the number of atomic antennas is at least twice the number of transmit antennas. This is because the  $N_r$  real-valued observations are sufficient to recover  $N_t \leq \frac{N_r}{2}$  complex-valued symbols. Consequently, under the same high SNR condition, the capacity gap between atomic MIMO and classic MIMO systems tends to a constant independent of SNR. In summary, to fully unleash the multiplexing gain of an atomic MIMO system, it is necessary to have  $N_r \geq 2N_t$ .

#### IV. IQ-AWARE DIGITAL PRECODING

When channel state information is available at both receiver and transmitter ends, we can manipulate the covariance matrix  $\bar{\mathbf{Q}}$  on purpose using precoding technique to achieve the instantaneous capacity in (13) for each channel realization. In this section, we propose an IQ-aware precoding approach designed to optimize digital precoding for atomic MIMO receivers. A comparison with traditional digital precoding is also presented for a comprehensive understanding.

##### A. Precoding architecture

We define  $\mathbf{s}_I \in \mathbb{R}^{N_s}$  and  $\mathbf{s}_Q \in \mathbb{R}^{N_s}$  as the transmitted symbols on the in-phase and quadrature (IQ) channels, respectively. The variable  $N_s$  represents the number of multiplexed data streams, which should be no larger than the number of maximum parallel spatial channels, i.e.,  $N_s \leq \min\{N_r/2, N_t\}$ . The overall baseband symbol is denoted as  $\bar{\mathbf{s}} = [\mathbf{s}_I^T, \mathbf{s}_Q^T]^T \in \mathbb{R}^{2N_s}$  in the real form and  $\mathbf{s} = \mathbf{s}_I + j\mathbf{s}_Q \in$

$\mathbb{C}^{N_s}$  in the complex form. The symbols  $\mathbf{s}_I$  and  $\mathbf{s}_Q$  follow an i.i.d Gaussian distribution  $\mathcal{N}(0, \frac{1}{2}\mathbf{I}_{N_s})$ . The objective of precoding is to design a linear mapping  $f: \bar{\mathbf{s}} \mapsto \bar{\mathbf{x}}$  such that the covariance matrix  $\bar{\mathbf{Q}}$  can maximize the mutual information  $\mathcal{I}(\mathbf{y}; \mathbf{x})$  as presented in (13).

To this end, we start with briefly reviewing the implementation of classical digital precoding. Classic MIMO systems widely adopt a complex-valued digital precoder  $\mathbf{F} = \mathbf{F}_I + j\mathbf{F}_Q \in \mathbb{C}^{N_t \times N_s}$  as depicted in Fig. 3 (a). The real-valued symbols  $\mathbf{s}_I$  and  $\mathbf{s}_Q$  are jointly processed by the two matrices  $\mathbf{F}_I$  and  $\mathbf{F}_Q$  on the digital baseband before entering the IQ modulator. After combining the IQ components, the transmitted signal in the complex form is thereby the complex product of  $\mathbf{F}$  and  $\mathbf{s}$ , specifically

$$\mathbf{x} = \mathbf{F}\mathbf{s} = \mathbf{F}_I\mathbf{s}_I - \mathbf{F}_Q\mathbf{s}_Q + j(\mathbf{F}_Q\mathbf{s}_I + \mathbf{F}_I\mathbf{s}_Q). \quad (16)$$

Because classical RF antennas can access both the real and imaginary parts of received signal, the complex-valued precoding is able to achieve the instantaneous capacity of classical MIMO by assigning  $\mathbf{F}$  with the principal singular vectors of the complex channel,  $\mathbf{H}$ . However, this method is infeasible for atomic MIMO systems. Specifically, to maximize the mutual information (13), it is necessary to expand the complex signal  $\mathbf{x}$  to the real form:

$$\bar{\mathbf{x}} = \begin{pmatrix} \mathbf{x}_I \\ \mathbf{x}_Q \end{pmatrix} = \underbrace{\begin{pmatrix} \mathbf{F}_I & -\mathbf{F}_Q \\ \mathbf{F}_Q & \mathbf{F}_I \end{pmatrix}}_{\mathbf{F}_r} \begin{pmatrix} \mathbf{s}_I \\ \mathbf{s}_Q \end{pmatrix}, \quad (17)$$

whose covariance matrix is  $\bar{\mathbf{Q}} = \frac{1}{2}\mathbf{F}_r\mathbf{F}_r^T$ . Due to the complex product relationship between  $\mathbf{F}$  and  $\mathbf{s}$  that produces  $\mathbf{x}$ , the equivalent linear mapping  $\mathbf{F}_r$  that constructs  $\bar{\mathbf{x}}$  has dependent diagonal and off-diagonal block components. This dependency makes it impossible to assign  $\mathbf{F}_r$  with the principal singular vectors of the real-valued channel  $\bar{\mathbf{H}}$  in (13). Thereby, the classical complex precoder is not suitable to the transmission model (8).

To address this issue, we propose to replace the conventional complex digital precoding with an *IQ-aware digital precoding* approach as presented in Fig. 3 (b). Unlike the joint manipulation of baseband symbols using the real and imaginary components of the complex precoder  $\mathbf{F}$ , our approach employs four real-valued matrices,  $\mathbf{F}_{k\ell} \in \mathbb{R}^{N_t \times N_s}$ ,  $k \in \{1, 2\}$ ,  $\ell \in \{1, 2\}$ , to independently process  $\mathbf{s}_I$  and  $\mathbf{s}_Q$ . By this means, the signals entering the IQ modulator become  $\mathbf{F}_{11}\mathbf{s}_I + \mathbf{F}_{12}\mathbf{s}_Q$  and  $\mathbf{F}_{21}\mathbf{s}_I + \mathbf{F}_{22}\mathbf{s}_Q$ , respectively. After combining these IQ components, the transmit signal in complex form is given as

$$\mathbf{x} = \mathbf{F}_{11}\mathbf{s}_I + \mathbf{F}_{12}\mathbf{s}_Q + j(\mathbf{F}_{21}\mathbf{s}_I + \mathbf{F}_{22}\mathbf{s}_Q), \quad (18)$$

while the real form is

$$\bar{\mathbf{x}} = \begin{pmatrix} \mathbf{x}_I \\ \mathbf{x}_Q \end{pmatrix} = \underbrace{\begin{pmatrix} \mathbf{F}_{11} & \mathbf{F}_{12} \\ \mathbf{F}_{21} & \mathbf{F}_{22} \end{pmatrix}}_{\bar{\mathbf{F}}} \begin{pmatrix} \mathbf{s}_I \\ \mathbf{s}_Q \end{pmatrix}. \quad (19)$$

Here,  $\bar{\mathbf{F}} \in \mathbb{R}^{2N_t \times 2N_s}$  is named the ‘‘IQ-aware digital precoder’’. Evidently, the complex signal  $\mathbf{x}$  in (18) is no longer the product of a complex-valued precoder and complex symbol,

like in (16). More importantly, the equivalent linear mapping  $\bar{\mathbf{F}}$  that generates  $\bar{\mathbf{x}}$  has independent block components, thereby imposing no additional constraints on the structure of covariance matrix  $\bar{\mathbf{Q}} = \frac{1}{2}\bar{\mathbf{F}}\bar{\mathbf{F}}^T$ . Henceforth, the proposed IQ-aware digital precoding offers more flexible manipulation to the radiated signal  $\mathbf{x}$  than the complex digital precoding. Therefore, it has the potential to achieve the instantaneous capacity of atomic receivers.

### B. Precoding method

We now seek an IQ-aware digital precoder that maximizes the mutual information. Let  $\bar{\mathbf{V}} \in \mathbb{R}^{2N_t \times 2N_t}$  denote the right-singular matrix of  $\bar{\mathbf{H}}$ , and let  $\{\bar{\lambda}_1, \dots, \bar{\lambda}_{\min\{N_r, 2N_t\}}\}$  represent the corresponding singular values of  $\bar{\mathbf{H}}$  in a descending order. According to the standard analysis of MIMO capacity, the optimal IQ-aware digital precoder  $\bar{\mathbf{F}}$  is given by:

$$\bar{\mathbf{F}} = \begin{pmatrix} \mathbf{F}_{11} & \mathbf{F}_{12} \\ \mathbf{F}_{21} & \mathbf{F}_{22} \end{pmatrix} = \bar{\mathbf{V}}_{:,1:2N_s} \bar{\mathbf{P}}^{\frac{1}{2}}. \quad (20)$$

The power allocation matrix  $\bar{\mathbf{P}} \triangleq \text{diag}\{\bar{p}_1, \dots, \bar{p}_{2N_s}\}$  is obtained using the water-filling principle:

$$\bar{p}_k = \left( \mu - \frac{\sigma^2}{\bar{\lambda}_k^2} \right)^+, \quad k \in \{1, \dots, 2N_s\}, \quad (21)$$

where the water level  $\mu$  is adjusted to satisfy the total power constraint  $\text{Tr}\{\bar{\mathbf{Q}}\} = \text{Tr}\{\bar{\mathbf{F}}\bar{\mathbf{F}}^T\} = \text{Tr}\{\bar{\mathbf{V}}_{:,1:2N_s} \bar{\mathbf{P}} \bar{\mathbf{V}}_{:,1:2N_s}^T\} = \sum_{k=1}^{2N_s} \bar{p}_k = P$ . Consequently, by processing baseband symbols  $\mathbf{s}_I$  and  $\mathbf{s}_Q$  using  $\{\mathbf{F}_{11}, \mathbf{F}_{12}, \mathbf{F}_{21}, \mathbf{F}_{22}\}$ , the system achieves its instantaneous capacity.

Last, by substituting  $\bar{\mathbf{F}}$  into (13), the achieved capacity of atomic MIMO systems, with  $N_s \leq \min\{N_r/2, N_t\}$ , is expressed as

$$C = \sum_{k=1}^{2N_s} \frac{1}{2} \log \left( 1 + \frac{\bar{\lambda}_k^2 \bar{p}_k}{\sigma^2} \right). \quad (22)$$

Then, we evaluate the asymptotic behavior of  $C$ . At high SNRs, the water-filling principle tends to allocate equal powers to all data streams, i.e.,  $\bar{p}_k = \frac{P}{2N_s}$ . Thereafter, the instantaneous capacity is asymptotically

$$C = N_s \log \frac{\text{SNR}}{N_s} + \sum_{k=1}^{2N_s} \frac{1}{2} \log \frac{\bar{\lambda}_k^2}{2}, \quad (\text{SNR} \rightarrow \infty). \quad (23)$$

Particularly, when the number of multiplexed data streams approaches the maximum parallel spatial channels, i.e.,  $N_s = \min\{N_r/2, N_t\}$ , the DoF of  $C$  is calculated to be  $\lim_{\text{SNR} \rightarrow \infty} \frac{C}{\log \text{SNR}} = \min\{N_r/2, N_t\}$ . This DoF is consistent with the analytical result of ergodic capacity, (15), without transmitter side CSI, demonstrating the effectiveness of the derived DoF.

## V. IQ-AWARE HYBRID PRECODING

In the preceding section, we have demonstrated that the capacity of atomic MIMO systems can be achieved using IQ-aware digital precoding. However, this solution presents additional challenges. Notably, optimal IQ-aware digital precoding



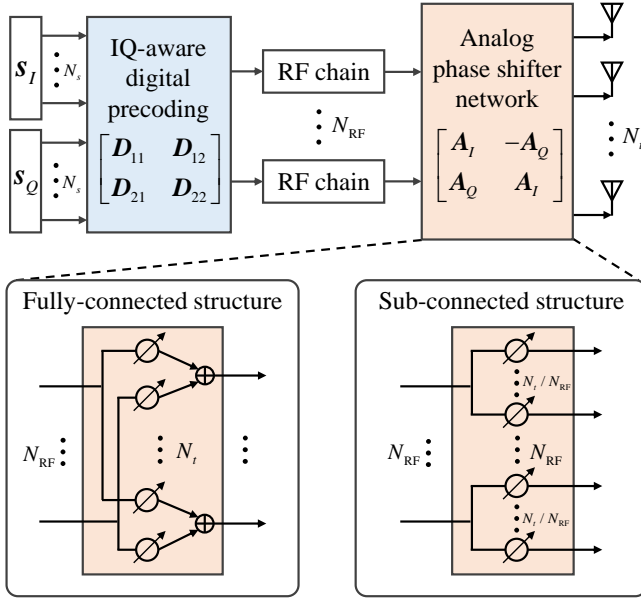


Figure 4. IQ-aware hybrid precoding with FC- and SC-PS networks.

has to manipulate the IQ symbols independently before the IQ modulator. This requirement mandates its implementation on a digital baseband processor, because analog circuits, like phase shifters and power amplifiers, cannot distinguish the combined IQ symbols. Consequently, our IQ-aware digital precoding approach necessitates a *fully digital precoding architecture*, where the number of RF chains is equal to the number of antennas. However, employing a large number of RF chains results in prohibitive hardware costs and power consumption, especially in massive MIMO systems. To mitigate these challenges, current 5G base stations (BSs) commonly adopt the *hybrid analog and digital precoding architectures*, presented in Fig. 4. For this architecture, precoding is executed by a low-dimensional digital processor followed by a high-dimensional analog PS network. In this typical scenario, the IQ-aware precoder proposed in (20) is clearly inapplicable due to its reliance on digital processing.

To tackle this challenge, we explore IQ-aware hybrid precoding in this section, incorporating a low-dimensional IQ-aware digital precoder in the baseband processor with an analog PS network in the RF front-end. These components are jointly optimized to approach the optimal IQ-aware digital precoder in (20). As illustrated in Fig. 4, our investigation focuses on two prevalent hybrid precoding architectures: the FC and SC PS networks [34].

#### A. IQ-Aware Hybrid Precoding with FC-PS Network

1) *Problem statement*: We first consider the IQ-aware hybrid precoding with a FC-PS network, where each RF chain is connected to all BS antennas via PSs. Denote the number of RF chains as  $N_{\text{RF}}$ , satisfying  $N_s \leq N_{\text{RF}} \ll N_t$ . In the baseband processor, an IQ-aware digital precoder  $\bar{\mathbf{D}}$  of dimension  $2N_{\text{RF}} \times 2N_s$  is employed, with block components  $\mathbf{D}_{k\ell} \in \mathbb{R}^{N_{\text{RF}} \times N_s}$ ,  $k \in \{1, 2\}$ ,  $\ell \in \{1, 2\}$ , to precode the symbols  $\mathbf{s}_I$  and  $\mathbf{s}_Q$ . The complex signal vector coming out

of RF chains is thus represented as  $\mathbf{s}_{\text{rf}} = \mathbf{D}_{11}\mathbf{s}_I + \mathbf{D}_{12}\mathbf{s}_Q + j(\mathbf{D}_{21}\mathbf{s}_I + \mathbf{D}_{22}\mathbf{s}_Q)$ . At the RF front-end, the analog precoder implemented by PSs is expressed by a complex matrix  $\mathbf{A} = \mathbf{A}_I + j\mathbf{A}_Q \in \mathbb{C}^{N_t \times N_{\text{RF}}}$ . Given that PSs can only adjust the phases of signals, each element of  $\mathbf{A}$  must satisfy the unit modulus constraint:  $|\mathbf{A}_{m,n}|^2 = \mathbf{A}_{I,m,n}^2 + \mathbf{A}_{Q,m,n}^2 = 1, \forall m, n$ . Thereafter, the transmitted signal  $\mathbf{x}$  is given as  $\mathbf{x} = \mathbf{A}\mathbf{s}_{\text{rf}}$ , whose real form is

$$\bar{\mathbf{x}} = \underbrace{\begin{pmatrix} \mathbf{A}_I & -\mathbf{A}_Q \\ \mathbf{A}_Q & \mathbf{A}_I \end{pmatrix}}_{\bar{\mathbf{A}}} \underbrace{\begin{pmatrix} \mathbf{D}_{11} & \mathbf{D}_{12} \\ \mathbf{D}_{21} & \mathbf{D}_{22} \end{pmatrix}}_{\bar{\mathbf{D}}} \underbrace{\begin{pmatrix} \mathbf{s}_I \\ \mathbf{s}_Q \end{pmatrix}}_{\bar{\mathbf{s}}}. \quad (24)$$

The covariance matrix of  $\bar{\mathbf{x}}$  is thus  $\bar{\mathbf{Q}} = \frac{1}{2}\bar{\mathbf{A}}\bar{\mathbf{D}}\bar{\mathbf{D}}^T\bar{\mathbf{A}}^T$ . Comparing precoding models (19) and (24), one can observe that the analog precoder  $\bar{\mathbf{A}}$  inherently possesses coupled diagonal and off-diagonal block components, which differentiates IQ-aware hybrid precoding from IQ-aware fully digital precoding.

To maximize the achievable rate, the analog precoder  $\bar{\mathbf{A}}$  and digital precoder  $\bar{\mathbf{D}}$  are jointly designed to approximate the optimal IQ-aware digital precoder  $\bar{\mathbf{F}}$ . Analogous to classical hybrid precoding design, we adopt the least-square principle to formulate the problem:

$$\min_{\bar{\mathbf{A}}, \bar{\mathbf{D}}} \|\bar{\mathbf{F}} - \bar{\mathbf{A}}\bar{\mathbf{D}}\|_F^2, \quad (25)$$

$$(P1) \quad \text{s.t.} \quad \mathbf{A}_{I,m,n}^2 + \mathbf{A}_{Q,m,n}^2 = 1, \forall m, n, \quad (25a)$$

$$\frac{1}{2}\text{Tr}\{\bar{\mathbf{A}}\bar{\mathbf{D}}\bar{\mathbf{D}}^T\bar{\mathbf{A}}^T\} = P, \quad (25b)$$

where (25b) is the total power constraint. Owing to the non-convex modulus constraint in (25a), the coupled components of  $\bar{\mathbf{A}}$ , as well as the product of  $\bar{\mathbf{A}}$  and  $\bar{\mathbf{D}}$ , directly solving problem (25) is challenging.

2) *Problem transformation*: To overcome these challenges, our first step is to seek an equivalent expression of (25) that decouples the analog precoder  $\bar{\mathbf{A}}$  from its multiplication with  $\bar{\mathbf{D}}$ , which can significantly simplify the precoding design.

Note that the columns of the optimal precoder  $\bar{\mathbf{F}}$  are mutually orthogonal to mitigate the interference between data streams. The designed hybrid precoder  $\bar{\mathbf{A}}\bar{\mathbf{D}}$  is thus expected to maintain column orthogonality as well. In massive MIMO systems,  $N_t \gg N_{\text{RF}}$ , the relationship  $\bar{\mathbf{A}}^T\bar{\mathbf{A}} \approx N_t\mathbf{I}_{2N_{\text{RF}}}$  holds with high probability [35]. This is because the diagonal elements of  $\bar{\mathbf{A}}^T\bar{\mathbf{A}}$  are exactly  $N_t$  while the off-diagonal elements can be approximated as the summation of  $2N_t$  independent terms, which is much less than  $N_t$  with high probability for  $N_t \gg 1$ . These properties imply that the columns of the optimal  $\bar{\mathbf{D}}$  are approximately orthogonal as well. Motivated by this observation, we introduce a column-orthogonal constraint on  $\bar{\mathbf{D}}$  and thereby replace it by  $\gamma\bar{\mathbf{D}}_u$ , where  $\bar{\mathbf{D}}_u^T\bar{\mathbf{D}}_u = \mathbf{I}_{2N_s}$  and  $\gamma$  is a normalization scalar to satisfy the total power constraint (25b). To determine the value of  $\gamma$ , we can substitute  $\bar{\mathbf{A}}^T\bar{\mathbf{A}} \approx N_t\mathbf{I}_{2N_{\text{RF}}}$  and  $\gamma\bar{\mathbf{D}}_u$  into (25b), thereby obtaining that  $\gamma \approx \sqrt{\frac{2P}{N_t}}$ . Consequently, the hybrid

precoding design problem is recast as

$$\min_{\bar{\mathbf{A}}, \bar{\mathbf{D}}_u} \|\bar{\mathbf{F}} - \gamma \bar{\mathbf{A}} \bar{\mathbf{D}}_u\|_F^2, \quad (26)$$

$$(P2) \quad \text{s.t.} \quad \mathbf{A}_{I,m,n}^2 + \mathbf{A}_{Q,m,n}^2 = 1, \quad \forall m, n, \quad (26a)$$

$$\bar{\mathbf{D}}_u^T \bar{\mathbf{D}}_u = \mathbf{I}_{2N_s}. \quad (26b)$$

Additionally, it is notable that although the columns of  $\bar{\mathbf{D}}_u \in \mathbb{R}^{2N_{\text{RF}} \times 2N_s}$  are orthogonal, its rows are typically nonorthogonal given that  $N_{\text{RF}} \geq N_s$ , making it intractable to decouple the product of  $\bar{\mathbf{A}}$  and  $\bar{\mathbf{D}}_u$ . To address this, we introduce two auxiliary matrices  $\bar{\mathbf{D}}_c \in \mathbb{R}^{2N_{\text{RF}} \times (2N_{\text{RF}} - 2N_s)}$  and  $\bar{\mathbf{F}}_c \in \mathbb{R}^{2N_t \times (2N_{\text{RF}} - 2N_s)}$ , which complement  $\bar{\mathbf{D}}_u$  to form a square matrix  $\tilde{\mathbf{D}} = (\bar{\mathbf{D}}_u, \bar{\mathbf{D}}_c) \in \mathbb{R}^{2N_{\text{RF}} \times 2N_{\text{RF}}}$  and complement  $\bar{\mathbf{F}}$  to form  $\tilde{\mathbf{F}} = (\bar{\mathbf{F}}, \bar{\mathbf{F}}_c) \in \mathbb{R}^{2N_t \times 2N_{\text{RF}}}$ , respectively. Then, the following lemma provides an equivalent expression for the objective function.

**Lemma 1.** *Given matrices  $\bar{\mathbf{F}} \in \mathbb{R}^{2N_t \times 2N_s}$ ,  $\bar{\mathbf{A}} \in \mathbb{R}^{2N_t \times 2N_{\text{RF}}}$ , and  $\bar{\mathbf{D}}_u \in \mathbb{R}^{2N_{\text{RF}} \times 2N_s}$  satisfying  $\bar{\mathbf{D}}_u^T \bar{\mathbf{D}}_u = \mathbf{I}_{2N_s}$  and  $N_t \gg N_{\text{RF}} \geq N_s$ , the following optimization problems are identical:*

$$\min_{\bar{\mathbf{A}}, \bar{\mathbf{D}}_u} \|\bar{\mathbf{F}} - \gamma \bar{\mathbf{A}} \bar{\mathbf{D}}_u\|_F^2 = \min_{\bar{\mathbf{A}}, \bar{\mathbf{D}}, \bar{\mathbf{F}}_c} \|\tilde{\mathbf{F}} - \gamma \bar{\mathbf{A}} \tilde{\mathbf{D}}\|_F^2, \quad (27)$$

where  $\tilde{\mathbf{F}} = (\bar{\mathbf{F}}, \bar{\mathbf{F}}_c) \in \mathbb{R}^{2N_t \times 2N_{\text{RF}}}$ ,  $\tilde{\mathbf{D}} = (\bar{\mathbf{D}}_u, \bar{\mathbf{D}}_c) \in \mathbb{R}^{2N_{\text{RF}} \times 2N_{\text{RF}}}$ , and  $\tilde{\mathbf{D}}^T \tilde{\mathbf{D}} = \tilde{\mathbf{D}} \tilde{\mathbf{D}}^T = \mathbf{I}_{2N_{\text{RF}}}$ .

*Proof:* (See Appendix C).  $\square$

Utilizing the auxiliary matrices, Lemma 1 converts the optimization of the column-orthogonal matrix  $\bar{\mathbf{D}}_u$  into optimizing the unitary matrix  $\tilde{\mathbf{D}}$ . Since a unitary transformation preserves the power of its input, we have

$$\|\tilde{\mathbf{F}} - \gamma \bar{\mathbf{A}} \tilde{\mathbf{D}}\|_F^2 = \|\tilde{\mathbf{F}} \tilde{\mathbf{D}}^T - \gamma \bar{\mathbf{A}}\|_F^2. \quad (28)$$

Comparing (25) and (28), it becomes evident that the analog precoder  $\bar{\mathbf{A}}$  no longer appears in the product form with the digital precoder  $\tilde{\mathbf{D}}$ . This simplification significantly facilitates our precoding algorithm design. By applying Lemma 1 and (28), problem (P2) is equivalently transformed into

$$\min_{\bar{\mathbf{A}}, \bar{\mathbf{D}}, \bar{\mathbf{F}}_c} \|\tilde{\mathbf{F}} \tilde{\mathbf{D}}^T - \gamma \bar{\mathbf{A}}\|_F^2 \quad (29)$$

$$(P3) \quad \text{s.t.} \quad \mathbf{A}_{I,m,n}^2 + \mathbf{A}_{Q,m,n}^2 = 1, \quad \forall m, n, \quad (29a)$$

$$\tilde{\mathbf{D}}^T \tilde{\mathbf{D}} = \tilde{\mathbf{D}} \tilde{\mathbf{D}}^T = \mathbf{I}_{2N_{\text{RF}}}. \quad (29b)$$

To efficiently solve this problem, we exploit the alternating minimization method, where the three variables  $\bar{\mathbf{A}}$ ,  $\tilde{\mathbf{D}}$ , and  $\bar{\mathbf{F}}_c$  are updated alternatively while keeping the others fixed until convergence. If the updated solutions in each iteration are all optimal, the alternating minimization method is guaranteed to converge to a local optimum, as elaborated in Section V-C.

3) *Algorithm design:* The step-by-step procedures of the proposed IQ-aware hybrid precoding algorithm for FC PSs are summarized in Algorithm 1, with detailed explanations provided below.

i) *Fix  $(\tilde{\mathbf{D}}, \bar{\mathbf{F}}_c)$  and optimize  $\bar{\mathbf{A}}$ :* We start by deriving the optimal solution for  $\bar{\mathbf{A}}$  after fixing matrices  $\tilde{\mathbf{D}}$  and  $\bar{\mathbf{F}}_c$ . We denote the block matrix components of  $\tilde{\mathbf{F}} \tilde{\mathbf{D}}^T$  as  $\mathbf{Z}_{kl} \in \mathbb{R}^{N_t \times N_{\text{RF}}}$ ,  $k \in \{1, 2\}$ ,  $\ell \in \{1, 2\}$ , such that

$$\tilde{\mathbf{F}} \tilde{\mathbf{D}}^T = \begin{pmatrix} \mathbf{Z}_{11} & \mathbf{Z}_{12} \\ \mathbf{Z}_{21} & \mathbf{Z}_{22} \end{pmatrix}. \quad (30)$$

**Algorithm 1:** IQ-aware hybrid precoding with FC-PS network

**Inputs:** The optimal IQ-aware fully digital precoder  $\bar{\mathbf{F}}$ .

1: Initialize  $\bar{\mathbf{F}}_c = \mathbf{0}$  and  $\bar{\mathbf{I}}_c = \mathbf{I}_{2N_{\text{RF}}}$ , and randomly initialize  $(\mathbf{A}_I, \mathbf{A}_Q)$ ;

2: Calculate  $\gamma = \sqrt{\frac{2P}{N_t}}$ ;

3: **while** not convergence **do**

4: Update  $\mathbf{A}_I$  and  $\mathbf{A}_Q$  by (33);

5: Compute the SVD,  $\tilde{\mathbf{F}}^T \bar{\mathbf{A}} = \mathbf{V}_1 \Sigma \mathbf{V}_2^T$ , and update  $\tilde{\mathbf{D}}$  by  $\mathbf{V}_2 \mathbf{V}_1^T$ ;

6: Update  $\bar{\mathbf{D}}_u = \tilde{\mathbf{D}}_{:,1:2N_s}$ ;

7: Update  $\bar{\mathbf{F}}_c = \gamma \bar{\mathbf{A}} \bar{\mathbf{D}}_{:,1+2N_s:2N_{\text{RF}}}$ ;

8: **end while**

9:  $\bar{\mathbf{D}} = \sqrt{\frac{2P}{\text{Tr}\{\bar{\mathbf{A}} \bar{\mathbf{D}}_u \bar{\mathbf{D}}_u^T \bar{\mathbf{A}}^T\}}} \bar{\mathbf{D}}_u$ ;

**Output:** Optimized precoder  $\bar{\mathbf{D}}$ ,  $\mathbf{A}_I$ , and  $\mathbf{A}_Q$ .

Then, the objective function can be rewritten as

$$\begin{aligned} \|\tilde{\mathbf{F}} \tilde{\mathbf{D}}^T - \gamma \bar{\mathbf{A}}\|_F^2 &= \left\| \begin{pmatrix} \mathbf{Z}_{11} - \gamma \mathbf{A}_I & \mathbf{Z}_{12} + \gamma \mathbf{A}_Q \\ \mathbf{Z}_{21} - \gamma \mathbf{A}_Q & \mathbf{Z}_{22} - \gamma \mathbf{A}_I \end{pmatrix} \right\|_F^2 \\ &= \|\mathbf{Z}_I - \gamma \mathbf{A}_I\|_F^2 + \|\mathbf{Z}_Q - \gamma \mathbf{A}_Q\|_F^2 + C_1 \\ &\propto \sum_{m=1}^{N_t} \sum_{n=1}^{N_{\text{RF}}} (\mathbf{Z}_{I,m,n} - \gamma \mathbf{A}_{I,m,n})^2 + (\mathbf{Z}_{Q,m,n} - \gamma \mathbf{A}_{Q,m,n})^2, \end{aligned} \quad (31)$$

where  $\mathbf{Z}_I \triangleq \mathbf{Z}_{11} + \mathbf{Z}_{22}$ ,  $\mathbf{Z}_Q \triangleq \mathbf{Z}_{21} - \mathbf{Z}_{12}$ , and  $C_1 = \gamma^2 \|\mathbf{A}_I\|_F^2 + \gamma^2 \|\mathbf{A}_Q\|_F^2 - 2\text{Tr}(\mathbf{Z}_{11}^T \mathbf{Z}_{22}) + 2\text{Tr}(\mathbf{Z}_{21}^T \mathbf{Z}_{12}) = \gamma^2 N_t N_{\text{RF}} - 2\text{Tr}(\mathbf{Z}_{11}^T \mathbf{Z}_{22}) + 2\text{Tr}(\mathbf{Z}_{21}^T \mathbf{Z}_{12})$ . Equations (31) and (29a) imply that the joint optimization of analog precoder is equivalent to independently optimizing each element of  $\mathbf{A} = \mathbf{A}_I + j\mathbf{A}_Q$ . Consider the PS connecting the  $m$ -th antenna and the  $n$ -th RF chain. The optimal precoder coefficient is obtained by solving

$$\min_{\mathbf{A}_{m,n}} \left( \frac{1}{\gamma} \mathbf{Z}_{I,m,n} - \mathbf{A}_{I,m,n} \right)^2 + \left( \frac{1}{\gamma} \mathbf{Z}_{Q,m,n} - \mathbf{A}_{Q,m,n} \right)^2 \quad (32)$$

$$(P4) \quad \text{s.t.} \quad \mathbf{A}_{I,m,n}^2 + \mathbf{A}_{Q,m,n}^2 = 1. \quad (32a)$$

Problem (P4) can be interpreted as finding a point  $(\mathbf{A}_{I,m,n}, \mathbf{A}_{Q,m,n})$  on the unit circle that is closest to  $(\frac{1}{\gamma} \mathbf{Z}_{I,m,n}, \frac{1}{\gamma} \mathbf{Z}_{Q,m,n})$ . The close-form solution is given as

$$\begin{cases} \mathbf{A}_{I,m,n}^* = \frac{\mathbf{Z}_{I,m,n}}{\sqrt{\mathbf{Z}_{I,m,n}^2 + \mathbf{Z}_{Q,m,n}^2}} \\ \mathbf{A}_{Q,m,n}^* = \frac{\mathbf{Z}_{Q,m,n}}{\sqrt{\mathbf{Z}_{I,m,n}^2 + \mathbf{Z}_{Q,m,n}^2}} \end{cases}, \quad (33)$$

which completes the update of  $\bar{\mathbf{A}}$  in step 4 of Algorithm 1.

ii) *Fix  $(\bar{\mathbf{A}}, \bar{\mathbf{F}}_c)$  and optimize  $\tilde{\mathbf{D}}$ :* With fixed matrices  $\bar{\mathbf{A}}$  and  $\bar{\mathbf{F}}_c$ , the objective function for optimizing  $\bar{\mathbf{D}}_u$  can be rewritten as

$$\begin{aligned} \|\tilde{\mathbf{F}} \tilde{\mathbf{D}}^T - \gamma \bar{\mathbf{A}}\|_F^2 &= \text{Tr}\{\tilde{\mathbf{F}}^T \tilde{\mathbf{F}} \tilde{\mathbf{D}}^T \tilde{\mathbf{D}}\} + \gamma^2 \text{Tr}\{\bar{\mathbf{A}}^T \bar{\mathbf{A}}\} - 2\gamma \text{Tr}\{\tilde{\mathbf{D}} \tilde{\mathbf{F}}^T \bar{\mathbf{A}}\} \\ &\stackrel{(a)}{=} \text{Tr}\{\tilde{\mathbf{F}}^T \tilde{\mathbf{F}}\} + 2N_t N_{\text{RF}} \gamma^2 - 2\gamma \text{Tr}\{\tilde{\mathbf{D}} \tilde{\mathbf{F}}^T \bar{\mathbf{A}}\}, \end{aligned} \quad (34)$$



where (a) holds because  $\tilde{\mathbf{D}}^T \tilde{\mathbf{D}} = \mathbf{I}_{2N_{\text{RF}}}$  and  $\text{Tr}\{\tilde{\mathbf{A}}^T \tilde{\mathbf{A}}\} = 2N_t N_{\text{RF}}$ . Thereafter, the optimal digital precoder  $\tilde{\mathbf{D}}$  is updated by solving

$$\max_{\tilde{\mathbf{D}}} \text{Tr}\{\tilde{\mathbf{D}} \tilde{\mathbf{F}}^T \tilde{\mathbf{A}}\} \quad (35)$$

$$(P5) \quad \text{s.t.} \quad \tilde{\mathbf{D}}^T \tilde{\mathbf{D}} = \mathbf{I}_{2N_{\text{RF}}}. \quad (35a)$$

Problem (P5) is a standard Orthogonal Procrustes Problem (OPP). To solve it, we compute the SVD of  $\tilde{\mathbf{F}}^T \tilde{\mathbf{A}}$  to obtain  $\mathbf{V}_1 \boldsymbol{\Sigma} \mathbf{V}_2^T$ . Then, (35) has the following upper bound:

$$\begin{aligned} \text{Tr}\{\tilde{\mathbf{D}} \tilde{\mathbf{F}}^T \tilde{\mathbf{A}}\} &= \text{Tr}\{\tilde{\mathbf{D}} \mathbf{V}_1 \boldsymbol{\Sigma} \mathbf{V}_2^T\} = \text{Tr}\{\mathbf{V}_2^T \tilde{\mathbf{D}} \mathbf{V}_1 \boldsymbol{\Sigma}\} \\ &= \sum_{n=1}^{2N_{\text{RF}}} (\mathbf{V}_2^T \tilde{\mathbf{D}} \mathbf{V}_1)_{n,n} \Sigma_{n,n} \stackrel{(b)}{\leq} \sum_{n=1}^{2N_{\text{RF}}} \Sigma_{n,n}, \end{aligned} \quad (36)$$

where (b) arises because the matrix  $\mathbf{V}_2^T \tilde{\mathbf{D}} \mathbf{V}_1$  is unitary. The equality holds if and only if  $\mathbf{V}_2^T \tilde{\mathbf{D}} \mathbf{V}_1 = \mathbf{I}_{2N_{\text{RF}}}$ . Thereafter,  $\tilde{\mathbf{D}}$  is updated by

$$\tilde{\mathbf{D}}^* = \mathbf{V}_2 \mathbf{V}_1^T. \quad (37)$$

Accordingly, the optimal digital precoder  $\tilde{\mathbf{D}}_u^*$  is determined by the first  $2N_s$  columns of  $\tilde{\mathbf{D}}^*$ :

$$\tilde{\mathbf{D}}_u^* = \tilde{\mathbf{D}}_{:,1:2N_s}^*, \quad (38)$$

which completes the update of digital precoder  $\tilde{\mathbf{D}}_u$  in steps 5 and 6.

iii) *Fix  $(\tilde{\mathbf{D}}, \tilde{\mathbf{A}})$  and optimize  $\tilde{\mathbf{F}}_c$* : We finally consider updating the auxiliary matrix  $\tilde{\mathbf{F}}_c$  given  $\tilde{\mathbf{D}}$  and  $\tilde{\mathbf{A}}$ . To this end, we explicitly express the the objective function  $\|\tilde{\mathbf{F}} - \tilde{\mathbf{A}} \tilde{\mathbf{D}}\|_F^2$  with respect to  $\tilde{\mathbf{F}}_c$  as

$$\|(\tilde{\mathbf{F}}, \tilde{\mathbf{F}}_c) - \gamma \tilde{\mathbf{A}} (\tilde{\mathbf{D}}_u, \tilde{\mathbf{D}}_c)\|_F^2 = \|\tilde{\mathbf{F}}_c - \gamma \tilde{\mathbf{A}} \tilde{\mathbf{D}}_c\|_F^2 + C_2, \quad (39)$$

where  $C_2 = \|\tilde{\mathbf{F}} - \gamma \tilde{\mathbf{A}} \tilde{\mathbf{D}}_u\|_F^2$  is irrelevant to  $\tilde{\mathbf{F}}_c$ . It is evident that the optimal  $\tilde{\mathbf{F}}_c$  needs to cancel the least square error introduced by  $\tilde{\mathbf{A}} \tilde{\mathbf{D}}_c$ :

$$\tilde{\mathbf{F}}_c^* = \gamma \tilde{\mathbf{A}} \tilde{\mathbf{D}}_c = \gamma \tilde{\mathbf{A}} \tilde{\mathbf{D}}_{:,1+2N_s:2N_{\text{RF}}}. \quad (40)$$

This completes the update of  $\tilde{\mathbf{F}}_c$  in step 7.

iv) *Power normalization*: Recall that the previously calculated  $\gamma$  is an approximated value. After the alternating minimization algorithm converges, we normalize the digital precoder  $\tilde{\mathbf{D}}_u$  by  $\sqrt{\frac{2P}{\text{Tr}\{\tilde{\mathbf{A}} \tilde{\mathbf{D}}_u \tilde{\mathbf{D}}_u^T \tilde{\mathbf{A}}^T\}}} \tilde{\mathbf{D}}_u$  to guarantee that the optimized precoders can perfectly satisfy the total power constraint. This completes the design of IQ-aware hybrid precoding with FC-PS structure.

## B. IQ-Aware Hybrid Precoding with SC-PS Network

1) *Problem statement*: We then investigate the SC-PS network. In this architecture, each RF is connected to a subset of the BS array with  $K = N_t/N_{\text{RF}}$  antennas. The number of required PSs is thus  $N_t$ . With much reduced PSs, the SC architecture exhibits lower spectral efficiency than the FC one, but is more energy-efficient and easier to implement in practice.

To simplify notation, we employ the same expressions for the digital precoder  $\tilde{\mathbf{D}}$  and analog precoder  $\tilde{\mathbf{A}}$  as used in

---

## Algorithm 2: IQ-aware hybrid precoding with SC-PS network

---

**Inputs:** The optimal IQ-aware fully digital precoder  $\bar{\mathbf{F}}$ .

- 1: Randomly initialize  $\mathbf{A}_I$ ,  $\mathbf{A}_Q$ , and  $\tilde{\mathbf{D}}$ .
- 2: **while** not convergence **do**
- 3:   Update  $\mathbf{A}_I$  and  $\mathbf{A}_Q$  by (46);
- 4:   Update  $\tilde{\mathbf{D}}$  by (48);
- 5: **end while**

**Output:** Optimized precoder  $\bar{\mathbf{D}}$ ,  $\mathbf{A}_I$ , and  $\mathbf{A}_Q$ .

---

Section V-A. The major difference lies in that  $\mathbf{A} = \mathbf{A}_I + j\mathbf{A}_Q$  is a block diagonal matrix in the SC-PS structure:

$$\mathbf{A} = \text{blkdiag}\{\mathbf{p}_1, \mathbf{p}_2, \dots, \mathbf{p}_{N_{\text{RF}}}\}, \quad (41)$$

where  $\mathbf{p}_n = [\exp(j\theta_{n,1}), \exp(j\theta_{n,2}), \dots, \exp(j\theta_{n,K})]^T$  represent the PSs connected to the  $n$ -th RF chain. One can verify that  $\mathbf{A}^H \mathbf{A} = K \mathbf{I}_{N_{\text{RF}}}$  and accordingly  $\bar{\mathbf{A}}^T \bar{\mathbf{A}} = K \mathbf{I}_{2N_{\text{RF}}}$  without difficulty. Bearing this property, the total power constraint is simplified to  $\frac{1}{2} \text{Tr}\{\bar{\mathbf{A}} \bar{\mathbf{D}} \bar{\mathbf{D}}^T \bar{\mathbf{A}}^T\} = \frac{K}{2} \text{Tr}\{\bar{\mathbf{D}} \bar{\mathbf{D}}^T\} = P$ . Henceforth, the precoding design problem is formulated as

$$\max_{\bar{\mathbf{A}}, \bar{\mathbf{D}}} \|\bar{\mathbf{F}} - \bar{\mathbf{A}} \bar{\mathbf{D}}\|_F^2 \quad (42)$$

$$(P6) \quad \text{s.t.} \quad \mathbf{A} = \text{blkdiag}\{\mathbf{p}_1, \mathbf{p}_2, \dots, \mathbf{p}_{N_{\text{RF}}}\}, \quad (42a)$$

$$\text{Tr}\{\bar{\mathbf{D}} \bar{\mathbf{D}}^T\} = 2P/K. \quad (42b)$$

Notably, the total power constraint is now independent of the analog precoder  $\bar{\mathbf{A}}$ . This fact enables us to directly utilize the alternating minimization approach to solve problem (P6).

2) *Algorithm design*: Similar to the FC algorithm, our SC hybrid precoding algorithm alternatively updates the analog and digital precoders while fixing the other one. The optimization details are presented below.

i) *Fix  $\bar{\mathbf{D}}$  and optimize  $\bar{\mathbf{A}}$* : Given  $\bar{\mathbf{D}}$ , we leverage matrix techniques to derive the optimal  $\bar{\mathbf{A}}$  that minimizes (42). By substituting  $\bar{\mathbf{A}}^T \bar{\mathbf{A}} = K \mathbf{I}_{2N_{\text{RF}}}$  into (42), the objective function is rewritten as

$$\|\bar{\mathbf{F}} - \bar{\mathbf{A}} \bar{\mathbf{D}}\|_F^2 = C_3 - 2 \text{Tr}\{\bar{\mathbf{D}} \bar{\mathbf{F}}^T \bar{\mathbf{A}}\}, \quad (43)$$

where  $C_3 = \text{Tr}\{\bar{\mathbf{F}}^T \bar{\mathbf{F}}\} + K \text{Tr}\{\bar{\mathbf{D}}^T \bar{\mathbf{D}}\}$ . To express (43) as a function of  $\mathbf{A}_I$  and  $\mathbf{A}_Q$  explicitly, we notice that the matrix  $\bar{\mathbf{A}}$  has an equivalent expression:

$$\begin{aligned} \bar{\mathbf{A}} &= \underbrace{\begin{pmatrix} \mathbf{I}_{N_t} & \mathbf{0} & \mathbf{0} & -\mathbf{I}_{N_t} \\ \mathbf{0} & \mathbf{I}_{N_t} & \mathbf{I}_{N_t} & \mathbf{0} \end{pmatrix}}_{\mathbf{U}} \begin{pmatrix} \mathbf{A}_I & \mathbf{0} \\ \mathbf{A}_Q & \mathbf{0} \\ \mathbf{0} & \mathbf{A}_I \\ \mathbf{0} & \mathbf{A}_Q \end{pmatrix} \\ &= \mathbf{U} \begin{pmatrix} \mathbf{A}_e & \mathbf{0} \\ \mathbf{0} & \mathbf{A}_e \end{pmatrix}, \end{aligned} \quad (44)$$

where  $\mathbf{A}_e \triangleq [\mathbf{A}_I^T, \mathbf{A}_Q^T]^T$ . Furthermore, let the block matrix components of  $\mathbf{U}^T \bar{\mathbf{F}} \bar{\mathbf{D}}^T$  be  $\mathbf{Y}_{k\ell} \in \mathbb{R}^{2N_t \times N_{\text{RF}}}$ ,  $k \in \{1, 2\}$ ,  $\ell \in \{1, 2\}$ . We can rewrite  $\text{Tr}\{\bar{\mathbf{D}} \bar{\mathbf{F}}^T \bar{\mathbf{A}}\}$  in (43) as

$$\begin{aligned} \text{Tr}\{\bar{\mathbf{D}} \bar{\mathbf{F}}^T \bar{\mathbf{A}}\} &= \text{Tr}\left\{\begin{pmatrix} \mathbf{Y}_{11}^T & \mathbf{Y}_{21}^T \\ \mathbf{Y}_{12}^T & \mathbf{Y}_{22}^T \end{pmatrix} \begin{pmatrix} \mathbf{A}_e & \mathbf{0} \\ \mathbf{0} & \mathbf{A}_e \end{pmatrix}\right\} \\ &= \text{Tr}\{(\mathbf{Y}_{11} + \mathbf{Y}_{22})^T \mathbf{A}_e\} \stackrel{(a)}{=} \text{Tr}\left\{(\mathbf{Y}_I, \mathbf{Y}_Q)^T \begin{pmatrix} \mathbf{A}_I \\ \mathbf{A}_Q \end{pmatrix}\right\} \\ &\stackrel{(b)}{=} \text{Tr}\{\text{Re}(\mathbf{Y}^H \mathbf{A})\} \stackrel{(c)}{\propto} -\frac{1}{2} \|\mathbf{Y} - \mathbf{A}\|_F^2, \end{aligned} \quad (45)$$

where (a) and (b) arise due to the definitions  $(\mathbf{Y}_I, \mathbf{Y}_Q) \triangleq \mathbf{Y}_{11} + \mathbf{Y}_{22}$  and  $\mathbf{Y} \triangleq \mathbf{Y}_I + j\mathbf{Y}_Q$ , and (c) holds by adding the constant  $-\frac{1}{2}(\|\mathbf{Y}\|_F^2 + \|\mathbf{A}\|_F^2)$  into  $\text{Tr}\{\text{Re}(\mathbf{Y}^H \mathbf{A})\}$ . The matrix transformations (43)-(45) successfully convert the primal objective function w.r.t  $\bar{\mathbf{A}}$  into a function w.r.t  $\mathbf{A}$ , which is independent of  $\bar{\mathbf{D}}$ . Thereafter, by further considering the block-matrix property of  $\mathbf{A}$  and the unit modulus constraint of PSs, the optimal phases  $\{\theta_{n,k}\}$  in precoder  $\mathbf{A}$  are given as

$$\theta_{n,k}^* = \arg \{ \mathbf{Y}_{(n-1)K+k,n} \}, \quad 1 \leq n \leq N_{\text{RF}}, 1 \leq k \leq K. \quad (46)$$

This completes the update of  $\mathbf{A}$ .

ii) *Fix  $\bar{\mathbf{A}}$  and optimize  $\bar{\mathbf{D}}$* : For a fixed analog precoder, the optimization of  $\bar{\mathbf{D}}$  is a quadratic programming problem with quadratic constraint. By applying the Karush-Kuhn-Tucker (KKT) conditions, the optimal solution is derived as

$$\bar{\mathbf{D}}^* = (\bar{\mathbf{A}}^T \bar{\mathbf{A}} + \lambda^* \mathbf{I}_{2N_{\text{RF}}})^{-1} \bar{\mathbf{A}}^T \bar{\mathbf{F}} = \frac{1}{K + \lambda^*} \bar{\mathbf{A}}^T \bar{\mathbf{F}}, \quad (47)$$

wherein the Lagrange multiplier  $\lambda^*$  is selected to fulfill the total power constraint. Accordingly, substituting (47) into (42b), we arrive at

$$\bar{\mathbf{D}}^* = \sqrt{\frac{2P}{K \|\bar{\mathbf{A}}^T \bar{\mathbf{F}}\|_F^2}} \bar{\mathbf{A}}^T \bar{\mathbf{F}}. \quad (48)$$

As a result, a step-by-step summary of the IQ-aware hybrid precoding algorithm for SC-PS structure is provided in Algorithm 2.

### C. Convergence and Complexity Analysis

1) *Convergence analysis*: For both Algorithms 1 and 2, the updated solutions in each iteration are all optimal to their respective sub-problems. Thereafter, our algorithms can monotonically decrease the objective functions  $\|\bar{\mathbf{F}}\tilde{\mathbf{D}}^T - \bar{\mathbf{A}}\|_F^2$  and  $\|\bar{\mathbf{F}} - \bar{\mathbf{A}}\tilde{\mathbf{D}}\|_F^2$ . Moreover, these two functions have a lower bound of zero. By invoking the monotone convergence theorem, the convergence of Algorithms 1 and 2 are guaranteed.

2) *Computational complexity analysis*: To evaluate the computational complexities of Algorithms 1 and 2, we access the number of scalar multiplications required by each algorithm.

To begin with, consider one iteration of Algorithm 1. Updating  $\mathbf{A}_I$  and  $\mathbf{A}_Q$  necessitates the calculation of matrices  $\mathbf{Z}_I$  and  $\mathbf{Z}_Q$ , which has a complexity of  $\mathcal{O}(N_t N_{\text{RF}}^2)$ . Next, the optimization of  $\tilde{\mathbf{D}}_u$  and  $\tilde{\mathbf{F}}_c$  involves the calculation of matrix  $\bar{\mathbf{F}}^T \bar{\mathbf{A}}$  and its SVD, resulting in a complexity on the order of  $\mathcal{O}(N_t N_{\text{RF}}^2 + N_{\text{RF}}^3)$ . In summary, the overall complexity of Algorithm 1 is  $\mathcal{O}(I_0(N_t N_{\text{RF}}^2 + N_{\text{RF}}^3))$ , where  $I_0$  is the number of iterations required for convergence.

In addition, consider one iteration of Algorithm 2. The complexity for updating  $\mathbf{A}_I$  and  $\mathbf{A}_Q$  primarily results from computing the expression of matrix  $\mathbf{Y}$ . This step has a complexity of  $\mathcal{O}(N_t N_{\text{RF}} N_s)$ . Subsequently, the complexity of updating  $\bar{\mathbf{D}}$  by (47) is on the order of  $\mathcal{O}(N_t N_{\text{RF}} N_s + N_{\text{RF}} N_s^2)$ . To summarize, the computational complexity of Algorithm 2 is  $\mathcal{O}(I_0(N_t N_{\text{RF}} N_s + N_{\text{RF}} N_s^2))$ .

## VI. SIMULATION RESULTS

### A. Simulation Settings

The default simulation settings are as follows. The Rydberg energy levels are set as  $62D_{5/2}$  and  $64P_{3/2}$  to measure  $\omega = 2\pi \times 27.7$  GHz radio frequency signals. The wavelength is  $\lambda = \frac{2\pi c}{\omega} = 10.83$  mm. Utilizing the Python package [36], the transition dipole moment  $\boldsymbol{\mu}_{eg}$  over the states  $62D_{5/2}$  and  $64P_{3/2}$  is calculated as  $[0, 789.107 q a_0, 0]^T$ , wherein  $a_0 = 5.292 \times 10^{-11}$  m specifies the Bohr radius and  $q = 1.602 \times 10^{-19}$  C is the charge of an electron. The atomic antennas are deployed as a uniform linear array (ULA) with an equal antenna spacing  $d = 10$  mm. The transmitter-to-receiver channel coefficients are generated using the standard Saleh-Valenzuela multi-path channel model. Specifically, the number of paths is set to  $L = 10$ . For each path, the complex coefficient  $\rho_{mnl} e^{j\varphi_{mnl}}$  is generated by the equation  $\rho_{mnl} e^{j\varphi_{mnl}} = \alpha_l e^{j\frac{\rho_{mnl} d \sin \vartheta_l}{\lambda}}$  according to the ULA geometry. Here, the path gain  $\alpha_l$  is sampled from the complex Gaussian distribution  $\mathcal{CN}(0, 1)$  and the incident angle  $\vartheta_l$  is sampled from the uniform distribution  $\mathcal{U}(-90^\circ, 90^\circ)$ . Besides, the polarization direction  $\epsilon_{nkl}$  is randomly sampled on a unit circle perpendicular to the incident angle. As for the LO-to-receiver channel, since the LO-to-receiver distance is quite small, we fix the path losses  $\{\rho_{R,m}\}$  as  $\rho_R$  and generate the phases  $\{\varphi_{R,m}\}$  from the distribution  $\mathcal{U}(0, 2\pi)$ . The SNR is defined as  $\frac{P}{\sigma^2}$ , while the receive SNR is defined as

$$\text{Receive SNR} = \frac{\mathbb{E}(\|\mathbf{H}\mathbf{x}\|_2^2)}{\mathbb{E}(\|\mathbf{n}\|_2^2)}. \quad (49)$$

To quantify the relative strength of the reference signal  $\mathbf{r}$ , we introduce the *reference-to-signal-and-noise ratio* (RSNR) defined as

$$\text{RSNR} = \frac{\mathbb{E}(\|\mathbf{r}\|_2^2)}{\mathbb{E}(\|\mathbf{H}\mathbf{x} + \mathbf{n}\|_2^2)}. \quad (50)$$

In our simulations, the parameters,  $\rho_R$ ,  $P$ , and  $\sigma^2$ , are properly adjusted to increase the receive SNR from -10 dB to 5 dB and the RSNR from -5 dB to 25 dB accordingly.

### B. DoF of Atomic Receivers

To begin with, the DoF of atomic MIMO receivers under high SNR regimes is evaluated in Fig. 5. We conduct 1000 Monte-Carlo trails to simulate the derivative of the ergodic capacity  $C_e$  w.r.t.  $\log \text{SNR}$ . The plotted curves include 1) the simulated DoF of a classic receiver when the phase of  $\mathbf{H}\mathbf{x} + \mathbf{r} + \mathbf{w}$  is known, whose DoF is theoretically  $\min\{N_t, N_r\}$ ; 2) the simulated DoF of an atomic receiver with a theoretical DoF of  $\min\{N_t/2, N_r\}$ ; and 3) the simulated DoF of in-phase transmission, where only the in-phase symbols,  $s_I$ , are transmitted and its theoretical DoF is  $\min\{N_t/2, N_r/2\}$ . The number of the transmit antennas is fixed as  $N_t = 2$ , while the number of receive antennas,  $N_r$ , grows from 2 to 4. We can observe from Fig. 5 that, with the increment of  $N_r$ , the DoF of an atomic receiver gradually climbs from 1 to 2. Thus, its capacity limit resembles the in-phase transmission when  $N_r = N_t = 2$  and becomes equivalent to the classic receiver when  $N_r = 2N_t = 4$ . This observation is consistent

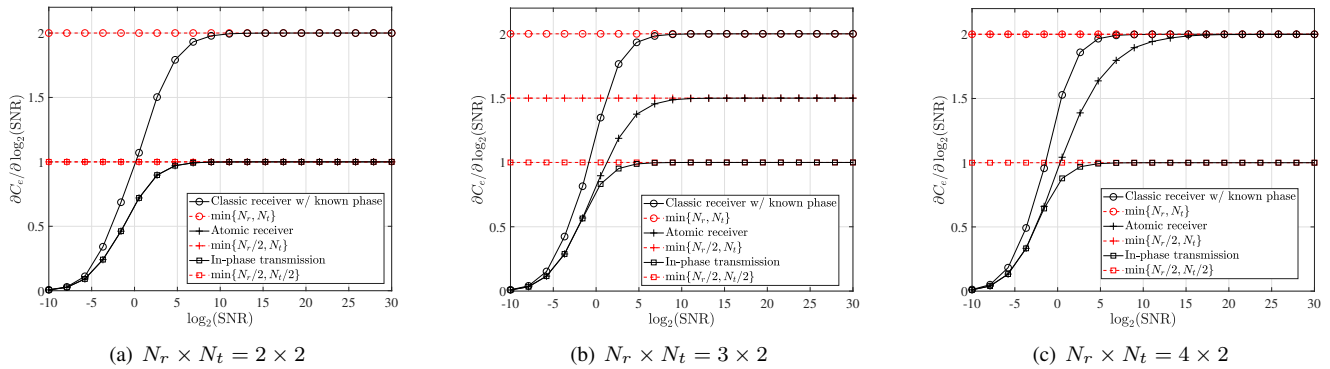


Figure 5. The derivative of the achievable rate  $C$  w.r.t  $\log_2(\text{SNR})$  under the (a)  $2 \times 2$  MIMO, (b)  $3 \times 2$  MIMO, and (c)  $4 \times 2$  MIMO configurations.

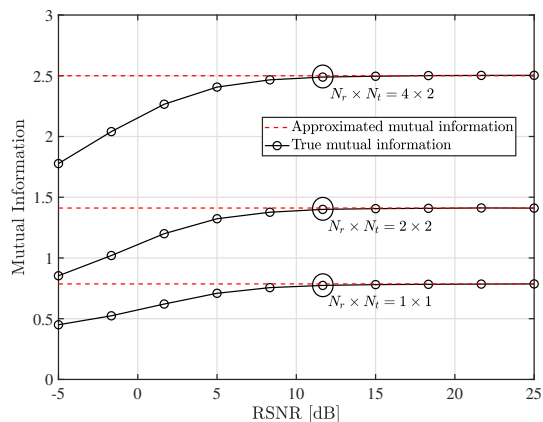


Figure 6. The mutual information between  $\mathbf{y}$  and  $\mathbf{x}$  against RSNR for the magnitude-detection model in (5) and real-part-detection model in (8).

with our analytical results in Section III. Even if an atomic receiver is hard to measure the phase of incident EM waves, it experiences no loss in DoF with the help of a strong reference signal and sufficient number of receive antennas. By further considering that the atomic receiver has a stronger sensitivity and thus has a much higher receive SNR, it has the potential to outperform the classic counterpart.

### C. Validation of Strong Reference Approximation

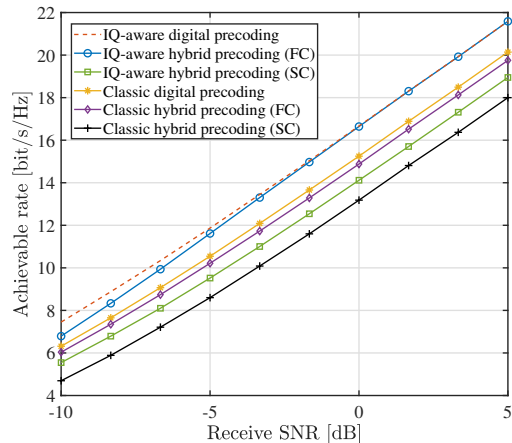
To validate the accuracy of the strong reference approximation, we plot the curves of the approximated mutual information,  $\mathcal{I}(\text{Re}(\tilde{\mathbf{H}}\mathbf{x}) + \mathbf{w}_I; \mathbf{x})$ , and the true mutual information,  $\mathcal{I}(\mathbf{y}; \mathbf{x})$ , derived from the nonlinear model (5). As presented in Fig. 6, three transmitter and receiver configurations are considered:  $N_r \times N_t = 1 \times 1, 2 \times 2$ , and  $4 \times 2$ . The RSNR grows from  $-5$  dB to  $25$  dB, while the receive SNR is fixed as  $0$  dB. Owing to the nonlinear input-output relationship,  $\mathcal{I}(\mathbf{y}; \mathbf{x})$  has no analytical expressions. Furthermore, calculating  $\mathcal{I}(\mathbf{y}; \mathbf{x})$  numerically involves the high-dimensional integration of non-central chi-square distribution, which is computationally prohibitive in practice. To address this issue, we adopt the Monte-Carlo method proposed in [37] to obtain  $\mathcal{I}(\mathbf{y}; \mathbf{x})$  numerically. As illustrated in Fig. 6, the true mutual information gradually converges to the approximated mutual information as RSNR increases. When RSNR is greater than  $10$  dB, the relative error

of mutual information is no more than  $1\%$ , which is accurate enough for practical approximation. Given that the LO-to-atomic-receiver distance is at the centimeter level, which is dozens of times shorter than the transmitter-to-atomic-receiver distance at the meter level, achieving a  $10$ -dB RSNR is feasible in practical scenarios. This validates the effectiveness of the strong reference approximation.

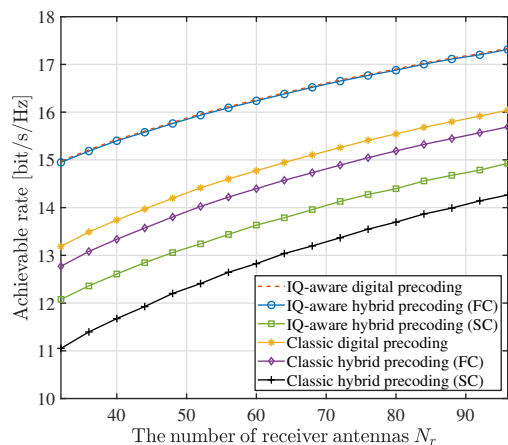
### D. Achievable Rate of Proposed Precoding Schemes

The curves in Fig. 7 compare different transmitter precoding approaches. The achievable rate of atomic MIMO receivers in (11) is adopted for performance evaluation. The benchmarks include: 1) the optimal IQ-aware digital precoding; 2-3) the proposed IQ-aware hybrid precoding for the FC- and SC-PS structures; 4) the classic digital precoding, which assigns the complex precoder  $\mathbf{F}$  with the principal singular vectors of the complex channel  $\tilde{\mathbf{H}}$  associated with water-filling principle; 5-6) the classic hybrid precoding algorithms, PE-AltMin for the FC structure and SDR-AltMin algorithm for the SC structure [34]. For both sub-figures, the number of data streams, RF chains, and transmit antennas are set to  $N_s = 3$ ,  $N_{\text{RF}} = 12$ , and  $N_t = 48$ . In Fig. 3 (a), the number of receive antennas is  $N_r = 72$  and the receive SNR grows from  $-10$  dB to  $5$  dB, while in Fig. 3 (b), the receive SNR is fixed as  $0$  dB and  $N_r$  increases from  $32$  to  $96$ . We run  $1000$  Monte-Carlo trails to plot each curve.

We can observe that all proposed IQ-aware precoding schemes outperform their traditional counterparts for all considered SNRs and the number of receive antennas. For example, when  $\text{SNR} = 0$  dB and  $N_r = 72$ , the gap in achievable rate is approximately  $2$  bit/s/Hz for the FC hybrid precoding architecture and around  $1$  bit/s/Hz for the SC hybrid precoding architecture, demonstrating the effectiveness of the proposed design. One can also observe that with the increase in SNR, the rate achieved by IQ-aware hybrid precoding (FC) gradually approaches that of the optimal IQ-aware digital precoding. This comes from the fact that the power allocation to the orthogonal columns of the digital precoder  $\mathbf{F}$  tend to be uniform at high SNRs, making the orthogonal-column assumption applied on  $\mathbf{D}$  more precise. Consequently, we can conclude that an analog FC-PS network associated with a low-



(a) Achievable rate vs Receive SNR



(b) Achievable rate vs Number of receive antennas

Figure 7. The achievable rate [bits/s/Hz] as a function of (a) the receive SNR [dB] and (b) the number of receive antennas,  $N_r$ .

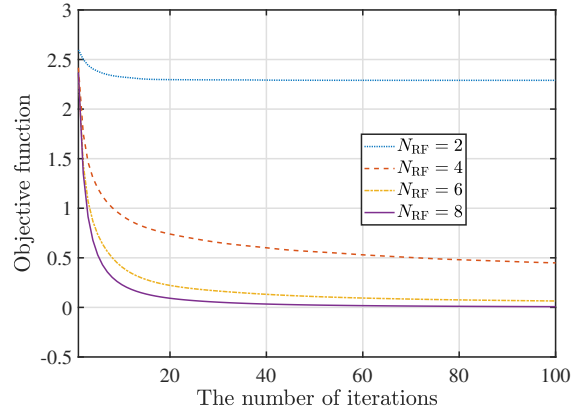
dimensional IQ-aware digital precoder is able to accurately approximate a high-dimensional IQ-aware digital precoder.

### E. Convergence Verification

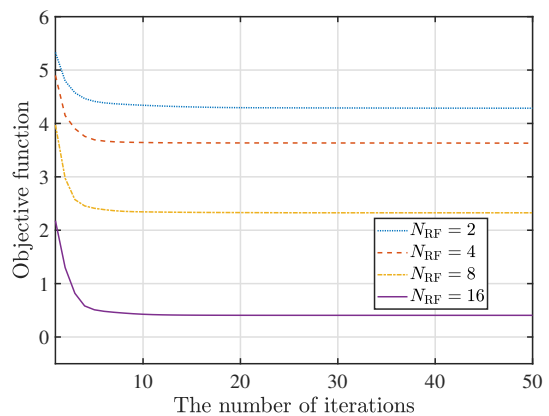
The curves in Fig. 8 demonstrate the convergence of Algorithm 1 and Algorithm 2. The value of objective functions,  $\|\tilde{\mathbf{F}}\tilde{\mathbf{D}}^T - \tilde{\mathbf{A}}\|_F^2$  and  $\|\tilde{\mathbf{F}} - \tilde{\mathbf{A}}\tilde{\mathbf{D}}\|_F^2$ , in each iteration are plotted in Fig. 8(a) and (b), respectively. The simulation parameters are as follows:  $N_s = 2$ ,  $N_t = 32$ ,  $N_r = 64$ , and SNR = 0 dB. It is clear that our proposed algorithms can monotonically decrease the objective functions until convergence. The number of iterations required for convergence is around 50 for Algorithm 1 and is around 10 for Algorithm 2. The larger iteration number of Algorithm 1 comes from the updating of auxiliary variables. Moreover, since the FC structure has much more PSs, the objective function of Algorithm 1 can converge to 0 when  $N_{RF} = 8$ , while the converged value of Algorithm 2 is larger than 0 when  $N_{RF} = 16$ .

## VII. CONCLUSION

In this paper, we explored transmitter precoding designs for approaching the capacity of Rydberg atomic receivers



(a) IQ-aware FC hybrid precoding



(b) IQ-aware SC hybrid precoding

Figure 8. The objective functions, (29) and (42), w.r.t the number of iterations.

in MIMO systems. We proposed a strong reference approximation to linearize the magnitude-detection model, effectively converting it into a real-part detector. Building on this, we established the limit of ergodic capacity as  $\min\{N_r/2, N_t\} \log\{\text{SNR}\} + \mathcal{O}(1)$ , such that a DoF-lossless transmission is enabled by atomic receivers when  $N_r \geq 2N_t$ . Then, we proposed an IQ-aware fully digital precoding to achieve the instantaneous capacity of atomic receivers, which offers more flexible manipulation on the IQ baseband symbols. To facilitate the implementation of analog RF circuits, we further delved into the IQ-aware hybrid precoding algorithms for both FC and SC architectures. Our simulation results confirmed that the proposed IQ-aware precoding schemes significantly outperform traditional precoding methods.

This work presents a significant stride towards the transmitter-side signal processing for enhancing atomic MIMO receivers. We conclude by outlining potential avenues for future research. Firstly, this study was limited to point-to-point MIMO systems. However, in the context of multi-user communications where each user utilizes an atomic receiver, it becomes crucial to consider inter-user interference. In such a scenario, the proposed precoding schemes may not be optimal. Secondly, our analyses and designs were built on the strong reference approximation. In case the LO is absent or the strong reference approximation is invalid, maximizing throughput for

the nonlinear transition model becomes necessary. This is still an open problem that requires further investigation.

## APPENDIX

### A. Proof of Proposition 1

The  $m$ -th entry of the received signal is given as

$$\begin{aligned} y_m &= |r_m + \mathbf{H}(m, :)\mathbf{x} + w_m| \\ &= |r_m| \sqrt{1 + \frac{|\mathbf{H}(m, :)\mathbf{x} + w_m|^2}{|r_m|^2} + 2\operatorname{Re}\left(\frac{\mathbf{H}(m, :)\mathbf{x} + w_m}{r_m}\right)} \\ &\stackrel{(a)}{\approx} |r_m| \left(1 + \operatorname{Re}\left(\frac{\mathbf{H}(m, :)\mathbf{x} + w_m}{r_m}\right) + \frac{|\mathbf{H}(m, :)\mathbf{x} + w_m|^2}{2|r_m|^2}\right) \\ &\stackrel{(b)}{=} |r_m| + \operatorname{Re}(e^{-j\angle r_m} \mathbf{H}(m, :)\mathbf{x}) + \operatorname{Re}(e^{-j\angle r_m} w_m), \end{aligned} \quad (51)$$

where (a) comes from the Taylor expansion  $\sqrt{1+x} = 1 + \frac{1}{2}x + \mathcal{O}(x^2)$  and (b) holds when  $|r_m| \gg |\mathbf{H}(m, :)\mathbf{x} + w_m|$ . Moreover, since  $\omega_n$  is circularly symmetric distributed, the rotation  $e^{-j\angle r_m}$  does not affect the distribution of  $\omega_m$ . Thereby,  $\operatorname{Re}(e^{-j\angle r_m} w_m)$  shares the same distribution with the real part of  $\omega_m$ , i.e.,  $\mathcal{N}(0, \sigma^2/2)$ . This completes the proof.

### B. Proof of Proposition 2

When  $\operatorname{SNR} \rightarrow +\infty$ , the ergodic capacity tends to  $\frac{1}{2}\mathbb{E}\left[\log \det\left(\frac{\operatorname{SNR}}{N_t} \bar{\mathbf{H}}\bar{\mathbf{H}}^T\right)\right] = \frac{1}{2}\mathbb{E}\left[\log \det\left(\frac{\operatorname{SNR}}{N_t} \bar{\mathbf{H}}^T \bar{\mathbf{H}}\right)\right]$ . We denote  $m = \min\{N_r/2, N_t\}$  and  $M = \max\{N_r/2, N_t\}$ , and further define

$$\mathbf{W} = \begin{cases} \bar{\mathbf{H}}\bar{\mathbf{H}}^T & \text{if } N_r \leq 2N_t \\ \bar{\mathbf{H}}^T \bar{\mathbf{H}} & \text{if } N_r > 2N_t \end{cases}. \quad (52)$$

Since the coefficients of  $\bar{\mathbf{H}} \in \mathbb{R}^{N_r \times 2N_t}$  follow the i.i.d Gaussian distribution  $\mathcal{N}(0, \frac{1}{2})$ ,  $\mathbf{W} \in \mathbb{R}^{2m \times 2m}$  has a Wishart distribution with  $2M$  degrees of freedom:  $\mathbf{W} \sim W_{2m}(\mathbf{V}, 2M)$ , where  $\mathbf{V} = \frac{1}{2}\mathbf{I}_{2m}$ . Substituting  $\mathbf{W}$  into the log-expectation expression of Wishart distribution [38], we arrive at

$$\begin{aligned} \frac{1}{2}\mathbb{E}\left[\log \det\left(\frac{\operatorname{SNR}}{N_t} \mathbf{W}\right)\right] &= m \log \frac{\operatorname{SNR}}{N_t} + \frac{1}{2}\mathbb{E}[\log \det(\mathbf{W})] \\ &= m \log \frac{\operatorname{SNR}}{N_t} + \frac{1}{2}\left(\log \left|\frac{1}{2}\mathbf{I}_{2m}\right| + 2m \log(2) + \psi_{2m}(M)\right) \\ &= m \log \frac{\operatorname{SNR}}{N_t} + \frac{1}{2}\psi_{2m}(M), \end{aligned} \quad (53)$$

where  $\psi_{2m}(M)$  denotes the multivariate digamma function (the logarithmic derivative of the multivariate gamma function). Since  $\frac{1}{2}\psi_{2m}(M)$  is a constant independent of SNR, the ergodic capacity is asymptotically  $\min\{N_r/2, N_t\} \log(\operatorname{SNR}/N_t) + \mathcal{O}(1)$  at high SNRs. This completes the proof.

### C. Proof of Lemma 1

The optimal solution of (27) is expressed as

$$\begin{aligned} &\min_{\bar{\mathbf{A}}, \bar{\mathbf{D}}, \bar{\mathbf{F}}_c} \|(\bar{\mathbf{F}}, \bar{\mathbf{F}}_c) - \gamma \bar{\mathbf{A}}(\bar{\mathbf{D}}_u, \bar{\mathbf{D}}_c)\|_F^2 \\ &= \min_{\bar{\mathbf{A}}} \left( \min_{\bar{\mathbf{D}}_u} \|\bar{\mathbf{F}} - \gamma \bar{\mathbf{A}}\bar{\mathbf{D}}_u\|_F^2 + \min_{\bar{\mathbf{F}}_c, \bar{\mathbf{D}}_c} \|\bar{\mathbf{F}}_c - \gamma \bar{\mathbf{A}}\bar{\mathbf{D}}_c\|_F^2 \right) \\ &\stackrel{(a)}{=} \min_{\bar{\mathbf{A}}, \bar{\mathbf{D}}_u} \|\bar{\mathbf{F}} - \gamma \bar{\mathbf{A}}\bar{\mathbf{D}}_u\|_F^2, \end{aligned} \quad (54)$$

where (a) holds by substituting  $\bar{\mathbf{F}}_c = \gamma \bar{\mathbf{A}}\bar{\mathbf{D}}_c$  into  $\|(\bar{\mathbf{F}}, \bar{\mathbf{F}}_c) - \gamma \bar{\mathbf{A}}\bar{\mathbf{D}}_c\|_F^2$ . This completes the proof.

## REFERENCES

- [1] A. Kaushik, R. Singh, S. Dayarathna, R. Senanayake, M. Di Renzo, M. Dajer, H. Ji, Y. Kim, V. Sciancalepore, A. Zappone, and W. Shin, "Toward integrated sensing and communications for 6G: Key enabling technologies, standardization, and challenges," *IEEE Commun. Standards Mag.*, vol. 8, no. 2, pp. 52–59, Jun. 2024.
- [2] J. Kraus, "Heinrich Hertz-theorist and experimenter," *IEEE Trans. Microw. Theory Techn.*, vol. 36, no. 5, pp. 824–829, 1988.
- [3] H. Nyquist, "Thermal agitation of electric charge in conductors," *Phys. Rev.*, vol. 32, no. 1, pp. 110–113, Jul. 1928.
- [4] J. A. Sedlacek, A. Schwettmann, H. Kübler, R. Löw, T. Pfau, and J. P. Shaffer, "Microwave electrometry with Rydberg atoms in a vapour cell using bright atomic resonances," *Nat. Phys.*, vol. 8, no. 11, pp. 819–824, Nov. 2012.
- [5] S. Kumar, H. Fan, H. Kübler, A. J. Jahangiri, and J. P. Shaffer, "Rydberg-atom based radio-frequency electrometry using frequency modulation spectroscopy in room temperature vapor cells," *Opt. Exp.*, vol. 25, no. 8, pp. 8625–8637, Apr. 2017.
- [6] H. Zhang, Y. Ma, K. Liao, W. Yang, Z. Liu, D. Ding, H. Yan, W. Li, and L. Zhang, "Rydberg atom electric field sensing for metrology, communication and hybrid quantum systems," *Sci. Bull.*, vol. 69, no. 10, pp. 1515–1535, May 2024.
- [7] C. T. Fancher, D. R. Scherer, M. C. S. John, and B. L. S. Marlow, "Rydberg atom electric field sensors for communications and sensing," *IEEE Trans. Quantum Eng.*, vol. 2, no. 3501313, pp. 1–13, Mar. 2021.
- [8] M. Saffman, T. G. Walker, and K. Mølmer, "Quantum information with Rydberg atoms," *Rev. Mod. Phys.*, vol. 82, no. 3, pp. 2313–2363, Aug. 2010.
- [9] C. J. Foot, *Atomic Physics*. Oxford University Press, 2005.
- [10] F. Zhang, B. Jin, Z. Lan, Z. Chang, D. Zhang, Y. Jiao, M. Shi, and J. Xiong, "Quantum wireless sensing: Principle, design and implementation," in *Proc. of Annu. Int. Conf. Mobile Comput. Netw. (ACM MobiCom'23)*, Oct. 2023, pp. 1–15.
- [11] M. Cai, S. You, S. Zhang, Z. Xu, and H. Liu, "Sensitivity extension of atom-based amplitude-modulation microwave electrometry via high Rydberg states," *Appl. Phys. Lett.*, vol. 122, no. 16, p. 161103, Apr. 2023.
- [12] J. Liu, Y. Shi, Z. M. Fadlullah, and N. Kato, "Space-Air-Ground Integrated Network: A Survey," *IEEE Commun. Surv. Tutor.*, vol. 20, no. 4, pp. 2714–2741, 2018.
- [13] D. A. Anderson, R. E. Sapiro, and G. Raithel, "An atomic receiver for AM and FM radio communication," *IEEE Trans. Antennas Propag.*, vol. 69, no. 5, pp. 2455–2462, May 2021.
- [14] J. Yuan, T. Jin, L. Xiao, S. Jia, and L. Wang, "A Rydberg atom-based receiver with amplitude modulation technique for the fifth-generation millimeter-wave wireless communication," *Antennas Wireless Propag. Lett.*, vol. 22, no. 10, pp. 2580–2584, Oct. 2023.
- [15] Z. Song, H. Liu, X. Liu, W. Zhang, H. Zou, J. Zhang, and J. Qu, "Rydberg-atom-based digital communication using a continuously tunable radio-frequency carrier," *Opt. Exp.*, vol. 27, no. 6, pp. 8848–8857, Mar 2019.
- [16] D. A. Anderson, R. E. Sapiro, and G. Raithel, "Rydberg atoms for radio-frequency communications and sensing: Atomic receivers for pulsed RF field and phase detection," *IEEE Aerosp. Electron. Syst. Mag.*, vol. 35, no. 4, pp. 48–56, 2020.
- [17] M. T. Simons, A. H. Haddab, J. A. Gordon, and C. L. Holloway, "A Rydberg atom-based mixer: Measuring the phase of a radio frequency wave," *Appl. Phys. Lett.*, vol. 114, no. 11, p. 114101, Mar. 2019.
- [18] C. L. Holloway, M. T. Simons, J. A. Gordon, and D. Novotny, "Detecting and receiving phase-modulated signals with a Rydberg atom-based receiver," *IEEE Antennas Wireless Propag. Lett.*, vol. 18, no. 9, pp. 1853–1857, Sep. 2019.
- [19] M. Jing, Y. H. Hu, J. Ma, H. Zhang, L. Zhang, L. Xiao, and S. Jia, "Atomic superheterodyne receiver based on microwave-dressed Rydberg spectroscopy," *Nat. Phys.*, vol. 1, pp. 911–915, Jun. 2020.
- [20] C. Holloway, M. Simons, A. H. Haddab, J. A. Gordon, D. A. Anderson, G. Raithel, and S. Voran, "A multiple-band Rydberg atom-based receiver: AM/FM stereo reception," *IEEE Antennas Propag. Mag.*, vol. 63, no. 3, pp. 63–76, Jun. 2021.
- [21] Y. Du, N. Cong, X. Wei, X. Zhang, W. Luo, J. He, and R. Yang, "Realization of multiband communications using different Rydberg final states," *AIP Adv.*, vol. 12, no. 6, p. 065118, Jun. 2022.

- [22] D. H. Meyer, J. C. Hill, P. D. Kunz, and K. C. Cox, "Simultaneous multiband demodulation using a rydberg atomic sensor," *Phys. Rev. Appl.*, vol. 19, p. 014025, Jan. 2023.
- [23] J. S. Otto, M. K. Hunter, N. Kjærgaard, and A. B. Deb, "Data capacity scaling of a distributed Rydberg atomic receiver array," *J. Appl. Phys.*, vol. 129, no. 15, p. 154503, Apr. 2021.
- [24] A. K. Robinson, N. Prajapati, D. Senic, M. T. Simons, and C. L. Holloway, "Determining the angle-of-arrival of a radio-frequency source with a Rydberg atom-based sensor," *Appl. Phys. Lett.*, vol. 118, no. 11, p. 114001, Mar. 2021.
- [25] D. Richardson, J. Dee, B. Kayim, B. Sawyer, R. Wyllie, R. T. Lee, and R. S. Westafer, "Study of angle of arrival estimation with linear arrays of simulated Rydberg atom receivers," *TechRxiv.24236953*, Apr. 2024.
- [26] M. Cui, Q. Zeng, and K. Huang, "Towards atomic MIMO receivers," *arXiv preprint arXiv:2404.04864*, Apr. 2024.
- [27] J. Dong, L. Valzania, A. Maillard, T.-a. Pham, S. Gigan, and M. Unser, "Phase retrieval: From computational imaging to machine learning: A tutorial," *IEEE Signal Process. Mag.*, vol. 40, no. 1, pp. 45–57, Jan. 2023.
- [28] E. Telatar, "Capacity of multi-antenna Gaussian channels," *Eur. Trans. Telecommun.*, vol. 10, no. 6, pp. 585–595, 1999.
- [29] L. Zheng and D. Tse, "Diversity and multiplexing: a fundamental tradeoff in multiple-antenna channels," *IEEE Trans. Inf. Theory*, vol. 49, no. 5, pp. 1073–1096, May 2003.
- [30] A. Artusio-Glimpse, M. T. Simons, N. Prajapati, and C. L. Holloway, "Modern RF measurements with hot atoms: A technology review of Rydberg atom-based radio frequency field sensors," *IEEE Microw. Mag.*, vol. 23, no. 5, pp. 44–56, May 2022.
- [31] M. Fox, *Quantum Optics: An Introduction*. Oxford University Press, 2006.
- [32] G. Chen, C. Wang, B. Yang, and T. Chen, "Instantaneous frequency estimation of radio frequency signal based on Rydberg atomic receiver," *IEEE Photonics J.*, vol. 16, no. 2, 2024.
- [33] D. Tse and P. Viswanath, *Fundamentals of Wireless Communication*. Cambridge University Press, 2005.
- [34] X. Yu, J.-C. Shen, J. Zhang, and K. B. Letaief, "Alternating Minimization Algorithms for Hybrid Precoding in Millimeter Wave MIMO Systems," *IEEE J. Sel. Top. Signal Process.*, vol. 10, no. 3, pp. 485–500, Apr. 2016.
- [35] O. E. Ayach, S. Rajagopal, S. Abu-Surra, Z. Pi, and R. W. Heath, "Spatially sparse precoding in millimeter wave MIMO systems," *IEEE Trans. Wireless Commun.*, vol. 13, no. 3, pp. 1499–1513, 2014.
- [36] N. Šibalić, J. Pritchard, C. Adams, and K. Weatherill, "Arc: An open-source library for calculating properties of alkali Rydberg atoms," *Comput. Phys. Commun.*, vol. 220, pp. 319–331, 2017.
- [37] G. Psaltopoulos and A. Wittneben, "Nonlinear MIMO: affordable MIMO technology for wireless sensor networks," *IEEE Trans. Wireless Commun.*, vol. 9, no. 2, pp. 824–832, Feb. 2010.
- [38] C. M. Bishop, *Pattern Recognition and Machine Learning*. Springer, 2006.